

A 2.5-dimensional viscous, resistive, advective magnetized accretion-outflow coupling in black hole systems: A higher order polynomial approximation. I

Shubhrangshu Ghosh

*Center for Astroparticle Physics and Space Science, Department of Physics,
Bose Institute, Block EN, Sector V, Salt Lake, Kolkata, India 700091*

The correlated and coupled dynamics of accretion and outflow around black holes (BHs) are essentially governed by the fundamental laws of conservation as outflow extracts matter, momentum and energy from the accretion region. Here we analyzed a robust form of 2.5-dimensional viscous, resistive, advective magnetized accretion-outflow coupling in BH systems, in the mean field magnetohydrodynamical (MHD) regime. We solve the complete set of coupled MHD conservation equations self-consistently, through invoking a generalized polynomial expansion in two dimensions. We perform a critical analysis of accretion-outflow region and provide a complete quasi-analytical family of solutions for advective flows. We obtain the physical plausible outflow solutions at high turbulent viscosity parameter α ($\gtrsim 0.3$), and at a reduced scale-height, as magnetic stresses compress or squeeze the flow region. We found that the value of the large-scale poloidal magnetic field \bar{B}_P is enhanced with increasing geometrical thickness of the accretion flow. On the other hand differential magnetic torque ($-r^2 \bar{B}_\varphi \bar{B}_z$) increases with the increase in \dot{M} . \bar{B}_P , $-r^2 \bar{B}_\varphi \bar{B}_z$ as well as the plasma beta β_P get strongly augmented with the increase in the value of α , enhancing the transport of vertical flux outwards. Our solutions indicate that magnetocentrifugal acceleration plausibly plays a dominant role in effusing out plasma from the radial accretion flow in moderately advective paradigm which are more centrifugally dominated, however in strongly advective paradigm it is likely that the thermal pressure gradient would play a more contributory role in the vertical transport of the plasma.

PACS numbers: 97.10.Gz, 97.60.Lf, 95.30.Qd, 98.62.Js, 98.58.Fd, 97.80.Jp

Keywords: Accretion and accretion disks, black holes, magnetohydrodynamics and plasmas, galactic nuclei, jets, X-ray binaries

I. INTRODUCTION

Outflows and jets are ubiquitous in nature. They are observed both in local universe, mostly in black hole (BH) X-ray binaries (BHXRBs) which are believed to harbour stellar mass BHs called microquasars [1], as well as in powerful extragalactic radio sources [2] where well-collimated outflows or jets emerge continuously from the nuclear region of the host active galaxies (AGNs) or quasars harbouring supermassive BHs. The accreting hot plasma around BHs powered by extreme gravity of the central object results in the formation of outflow/jet which extracts mass, angular momentum and energy from the inner regions of the accretion flow. The outflows in microquasars are observed only in low-hard state of BHXRBs [3,4] which are radiatively inefficient. Radiatively inefficient accretion flows (RIAFs) are hot gas pressure dominated systems which are geometrically thick ($h(r)/r \gtrsim 0.1$) and optically thin, where $h(r)$ is the scale-height of the accretion region. The dynamics of the flow is thus strongly sub-Keplerian and advection dominated [5,6]. RIAFs occur when the mass accretion rate \dot{M} is very low (presumably with $\dot{M} \lesssim 10^{-3} \dot{M}_{\text{Edd}}$), where \dot{M}_{Edd} is the Eddington accretion rate or the accretion rate corresponding to the Eddington luminosity. Outflows/jets are not likely observed in high-soft state of BHXRBs ([4] and references therein), which are believed to be powered by geometrically thin and optically thick radiation pressure dominated Keplerian accretion disk [7].

Theoretically speaking, it has been argued [5,8,9,10] that a geometrically thick advective accretion flow has a strong tendency to drive bipolar outflows due to high thermal energy content of the hot gas. They may be additionally propitious to propel outflows/jets because its vertical thick structure enhances the large-scale poloidal component of the magnetic field, which plays a critical role in launching strong and collimated outflows [11].

Apart from low-hard state of BHXRBs which power jets, at the other end of the spectrum, strong outflows and jets are observed in low excitation radio galaxies (LERGs) harbouring supermassive BHs. LERGs, a more generalization of low luminous AGNs (LLAGNs) seem to be accreting gaseous plasma directly from the hot X-ray emitting phase of interstellar medium (ISM) or from the hot X-ray halos surrounding the galaxy or from the hot phase of the intergalactic medium (IGM) quasi-spherically in a radiatively inefficient mode with near Bondi rate [12]. LERGs thus resemble low-hard state of BHXRBs having geometrically thick and optically thin gas pressure dominated strongly advective quasi-spherical accretion flow, accreting hot gas at a high sub-Eddington accretion rate (presumably with $\dot{M} \lesssim 10^{-3} \dot{M}_{\text{Edd}}$). This strongly advective radiatively inefficient accretion paradigm (RIAF) or hot mode accretion having considerable geometrical thickness, is more prone to emanate outflows/jets and is very conducive to propel

matter vertically outwards out of the accreting region.

However, with the increase in \dot{M} as $10^{-3}\dot{M}_{\text{Edd}} \ll \dot{M} \lesssim 10^{-2}\dot{M}_{\text{Edd}}$, the flow tends to be more centrifugally dominated and become moderately advective, with the central BH accreting relatively cold gas as compared to the hot mode accretion. Incidentally the moderately advective accretion flow does not occur in a radiatively inefficient mode, but where considerable amount of both gas and radiation pressure seem to be present in the system, rendering the flow to have a moderate optical depth. Geometrically, the inner advective region would then be relatively thinner than that correspond to RIAFs. The moderately advective accretion paradigm may also be susceptible to eject outflows. The difference between this paradigm and with the RIAF, however, may lie in the acceleration mechanisms to eject bipolar outflows and jets, which we would eventually investigate in this study. Nonetheless, with the increase in \dot{M} as the flow tends to become more rotationally/centrifugally dominated with lesser geometrical thickness, the efficacy of the disk to eject outflows diminishes. Beyond $\dot{M} > 10^{-2}\dot{M}_{\text{Edd}}$, the flow would eventually tend towards Keplerian nature ([13]; paper II (in preparation)). Geometrically thin Keplerian accretion disk plausibly fails to account for the launching and acceleration of outflows and jets ([8,9,10]; also see [14] for further discussion).

Extensive work has been pursued on the origin of outflow/jet, since the seminal work of Blandford & Payne [15] in studying accretion powered hydromagnetic outflows, which we like to focus upon in this study. Physical understanding of the accretion powered hydromagnetic outflows have either been performed in stationary self-similar approximation [15,16,17] in quasi-analytical regime to demonstrate the importance of poloidal component of the magnetic field to launch outflowing matter from the Keplerian accretion disk, or through magnetohydrodynamic (MHD) simulations in both nonrelativistic as well as in relativistic regimes (For details, see the introduction in [8,10] and references therein, also see [18] and references therein). In most of these studies the authors remain focused mainly on the launching of outflows/jets from the geometrically thin Keplerian disk. The formation of the accretion powered outflow and jet is directly related to the efficacy of extraction of angular momentum and energy from the magnetized accretion flow. However, the exact mechanism by which the radial accretion is diverted into strong outflows and plausible jets still remains theoretically elusive. Notwithstanding, jet launching is completely a magnetohydrodynamic process. Accreting material diffuses across magnetic field lines threading the accretion region, is then lifted upwards by MHD forces which then couples to the field and becomes accelerated magnetocentrifugally. However, if the accreting system is strongly gas pressure dominated, it may happen that the gas pressure gradient would play a more contributory role to lift the plasma vertically outwards along with the help of magnetic forces. In addition, turbulent reconnection of magnetic field lines may lead to flux annihilation [19]. Magnetic energy dissipates through turbulent magnetic reconnection, may also power the outflow/jet emission ([20] and references therein).

Most of the studies of accretion disk and outflow/jet have evolved separately, assuming these two to be apparently dissimilar objects. In the light of both deeper theoretical understanding and observational inferences [21,22,3] it is evident that the dynamics of outflow and the underlying accretion are strongly correlated (for details see [8,9,10] and references therein). Outflows and jets observed in AGNs and XRBs can only originate in an accretion powered system, where the accreting plasma around gravitating objects like BHs acts as a source, whereas outflow and then jet acts as one of the possible sinks [10]. The implicit coupling between accretion and outflow is then essentially governed by conservation laws; conservation of matter, momentum and energy. The outflowing matter carries away mass, angular momentum and energy extracted from the accreting plasma [16]. We do not intend to investigate the physics of jet formation and its launching mechanism which is altogether a different field of research, but would like to focus entirely on the inter-correlating dynamics of the accretion and outflow within the coupled accretion-outflow region, and the conditions/criteria for jet launching. Any proper understanding of the dynamics and the conditions of jet launching should necessarily require the robust understanding of the dynamics of the magnetized advective accretion region coupled to outflow, governed explicitly by the conservation laws. The relevant dynamical solutions at the accretion-outflow coupled surface (the surface from where outflow decouples from radially inward accretion flow) would then act as boundary conditions at the base of the jet.

Accretion disk-outflow/jet coupling has been studied on number of occasions from purely observational angle, in accretion powered systems [22,23]. From theoretical perspective, few self-similar studies have been attempted in the context to accretion-outflow coupling, both in non magnetized and in magnetized regime (see [18] and references therein; [8,9,10,24,25,26]). Notwithstanding, theoretically, it is still difficult to construct reasonably satisfactory and definitive model of magnetized accretion-outflow/jet coupled region, owing to the complicated geometry and inconclusive understanding of the inflow-outflow coupled region. On the other hand, few simulations on disk-outflow/jet coupling have also been cultivated [27,28,29]. In these simulations how the matter gets deflected from the equatorial plane has been studied largely in the Keplerian regime. Casse and Keppens [30] performed an advective, resistive MHD simulation of accretion-ejection structure with the inclusion of the energy equation, however neglecting the viscosity and radiative loss from the system. Nonetheless, it is still difficult to simultaneously simulate the accretion and the outflow regions because the time scales of the accretion and outflow are in general very different.

In the present work, we endeavour to develop a robust viscous, resistive and advective MHD accretion-induced outflow model in the 2.5 dimensional regime, in the mean field MHD approximation, in the context to accretion powered hydromagnetic outflows/jets, focusing entirely on the inter-correlating dynamics of the accretion and outflow within the coupled accretion-outflow region, without aspiring to explore the mechanism of launching and ejection of outflows and jets. A complete 2.5-dimensional viscous, resistive, advective global MHD numerical solution of such a system is left for further work, and which is beyond the scope at present; we confine our treatment to quasi-analytical/quasi-numerical power law self-similarity (e.g., [5]) in a quasi-stationary configuration, by upholding the conservation equations. All physical quantities are scaled as powers in r and z according to their dimensions, in the limit of higher order polynomial expansion. We will perform a critical analysis of accretion-outflow region and provide a complete quasi-analytical family of solutions. Although the quasi-analytical self-similar solutions are approximate, they, however, can provide a strong physical intuitive picture of accretion dynamics coupled with the outflow, as well as physical criteria/conditions to eject outflows/jets. In the next section, we present the formulation of our model. §III describes the quasi-analytical/quasi-numerical procedure to solve the model equations of the accretion-induced outflow. In §IV, we evaluate the coefficients of our self-similar solutions and analyze them. In §V, we investigate the nature and behaviour of the family of solutions for accretion-induced outflow within the bounded accretion coupled outflow region. Finally, we end up in §VI with a summary and discussion.

II. 2.5-DIMENSIONAL ADVECTIVE ACCRETION-OUTFLOW COUPLING IN THE MEAN-FIELD MHD REGIME

We formulate the accretion-outflow coupled model by considering a 2.5-dimensional viscous, resistive, advective accretion flow geometry in the mean field MHD regime as strong outflows/jets are more likely to eject from a geometrically thick, advective region of the accretion flow. The vertical flow is explicitly included in the system. We adopt the cylindrical coordinate system (r, φ, z) to describe a quasi-stationary, mean axisymmetric accretion flow. As we have incorporated outflow in our system, within the accretion-outflow coupled region in advective paradigm, all the dynamical flow variables; namely, radial velocity (v_r), azimuthal velocity (v_φ), specific angular momentum (λ), vertical velocity or outflow velocity (v_z), isothermal sound speed (c_s), mass density (ρ), thermal pressure (P) and magnetic field components (B_r, B_z, B_φ) vary in both r and z . The dynamical equations are vertically integrated over an arbitrary scale height $h(r)$ from $-h$ to $+h$. Here $h(r)$ is not a hydrostatic disk-scale height but a photospheric surface within which accretion and outflow are coupled. Above $h(r)$, the outflow decouples from the accretion flow, gets further accelerated in the hot nonthermal magnetized corona and finally forms a relativistic jet. We focus on this accretion-outflow coupled region within which the flow is mostly bounded. We only include the $r\varphi$ component of turbulent stress, which is responsible for radial transport of angular momentum outwards (angular momentum get transported due to the diffusion of turbulent eddies). Vertical transport of angular momentum occurs mainly through large-scale magnetic stresses, where the outflowing matter magnetically extracts or removes angular momentum. The accreting mass is assumed to be much less as compared to that of the central object, and hence the flow is not self-gravitating. As the accretion flow is inherently turbulent, we express all the dynamical variables in mean and fluctuating part. Microscopic viscosity and resistivity are neglected compared to the large-scale diffusion of turbulent eddies. Assuming that the fluctuation in the density is very less; in the limit of Boussinesq approximation, the generic ansatz follows as

$$F = \bar{F} + F', \quad \overline{F'} = 0, \quad \frac{\rho'}{\bar{\rho}} \ll 1, \quad (1)$$

where \bar{F} represents the mean flow which is either a time average or an ensemble average. F' is then the fluctuation corresponding to that variable. The turbulence is defined in terms of mean Reynolds and Maxwell stress described through correlations given by

$$\bar{t}_{ij} = \overline{t_{ij}^{\mathcal{R}}} + \overline{t_{ij}^{\mathcal{M}}} \Rightarrow - \left[\overline{\rho v'_i v'_j} - \left(\frac{\overline{B'_i B'_j}}{4\pi} - \delta_{ij} \frac{\overline{B'^2}}{8\pi} \right) \right], \quad (2)$$

where, \bar{t}_{ij} is the net turbulent stress. Statistical averaging of MHD equations generates large number of turbulent correlation terms. In the present study, we restrict to first order turbulent correlation and neglect second order and higher order correlation terms. The Reynolds and Maxwell stresses are commonly parameterized in terms of kinetic and magnetic turbulent viscosities $\nu_{ij}^{\mathcal{R}}$ and $\nu_{ij}^{\mathcal{M}}$ respectively as

$$\overline{\rho v'_i v'_j} = -\nu_{ij}^{\mathcal{R}} \bar{\rho} \bar{s}_{ij}, \quad (3)$$

$$-\left(\frac{\overline{B'_i B'_j}}{4\pi} - \delta_{ij} \frac{\overline{B'^2}}{8\pi}\right) = -\nu_{ij}^{\mathcal{M}} \bar{\rho} \bar{s}_{ij}, \quad (4)$$

where $\bar{s}_{ij} = \frac{\partial \bar{v}_i}{\partial x_j} + \frac{\partial \bar{v}_j}{\partial x_i} - \frac{2}{3} \nabla \cdot \bar{\mathbf{v}} \delta_{ij}$ is the strain tensor. The turbulent viscosities are parameterized through an α prescription as

$$\nu_{ij}^{\mathcal{R}} \sim \alpha_{ij}^{\mathcal{R}} \bar{c}_s h, \quad \nu_{ij}^{\mathcal{M}} \sim \alpha_{ij}^{\mathcal{M}} \bar{c}_s h, \quad (5)$$

where $\nu_{ij} = \nu_{ij}^{\mathcal{R}} + \nu_{ij}^{\mathcal{M}}$ is the net turbulent viscosity and $\alpha_{ij} = \alpha_{ij}^{\mathcal{R}} + \alpha_{ij}^{\mathcal{M}}$ is the net turbulent viscosity parameter. With these parameterizations, the coupled accretion-outflow dynamical equations in quasi-stationary state are as follows:

(a) Mass transfer:

$$\frac{\partial(\bar{\rho} \bar{v}_j)}{\partial x_j} = 0. \quad (6)$$

We define the net mass flow rate which is a constant, through an integro-differential equation as

$$\int_{-h}^{+h} \int_r \int_0^{2\pi} \left[\frac{1}{r} \frac{\partial}{\partial r} (r \bar{\rho} \bar{v}_r) + \frac{\partial}{\partial z} (\bar{\rho} \bar{v}_z) \right] r d\varphi dr dz = -\dot{M}, \quad (7)$$

where the first term is the signature of the radial accretion flow and the second term attributes to outflow. If we discard \bar{v}_z (neglecting outflow), Eqn. (7) reduces to a height integrated continuity equation of the accretion flow, and where \dot{M} would then be the usual mass accretion rate.

(b) Momentum transfer:

The momentum balance equation in the mean field MHD is given by

$$\frac{\partial(\bar{\rho} \bar{v}_i \bar{v}_j)}{\partial x_j} = -\bar{\rho} \frac{\partial \varphi_G}{\partial x_i} - \frac{\partial \bar{p}}{\partial x_i} + \frac{\partial}{\partial x_j} \left(\frac{\bar{B}_i \bar{B}_j}{4\pi} - \delta_{ij} \frac{\bar{B}^2}{8\pi} \right) + \frac{\partial}{\partial x_j} \left(\bar{t}_{ij}^{\mathcal{R}} + \bar{t}_{ij}^{\mathcal{M}} \right). \quad (8)$$

Using Eqn. (6) and integrating Eqn. (8) vertically, the radial momentum balance equation is given by

$$\int_{-h}^{+h} \left[\bar{\rho} \bar{v}_r \frac{\partial \bar{v}_r}{\partial r} - \bar{\rho} \frac{\bar{\lambda}^2}{r^3} + \bar{\rho} \bar{v}_z \frac{\partial \bar{v}_r}{\partial z} + \bar{\rho} F_{Gr} + \frac{\partial \bar{P}}{\partial r} + \frac{1}{4\pi} \left(\frac{\bar{B}_\varphi}{r} \frac{\partial}{\partial r} (r \bar{B}_\varphi) + \bar{B}_z \frac{\partial \bar{B}_z}{\partial r} - \bar{B}_r \frac{\partial \bar{B}_r}{\partial z} \right) \right] dz = 0. \quad (9)$$

In deriving this we have used divergence criteria of magnetic field. F_{Gr} is the radial component of the gravitational force. In a similar fashion, we write the azimuthal momentum balance equation as

$$\int_{-h}^{+h} \left(\bar{\rho} \frac{\bar{v}_r}{r} \frac{\partial \bar{\lambda}}{\partial r} + \bar{\rho} \frac{\bar{v}_z}{r} \frac{\partial \bar{\lambda}}{\partial z} \right) dz = \frac{1}{r^2} \frac{\partial}{\partial r} \int_{-h}^{+h} \left(r^2 \bar{t}_{r\varphi} \right) dz + \int_{-h}^{+h} \frac{1}{r^2} \frac{\partial}{\partial r} \left(\frac{r^2 \bar{B}_r \bar{B}_\varphi}{4\pi} \right) dz + \frac{\bar{B}_\varphi \bar{B}_z}{4\pi} \Big|_{-h}^{+h}. \quad (10)$$

The last term in the right hand side of Eqn. (10) is the magnetic torque that acts at the accretion-outflow surface, and which helps in transporting the angular momentum vertically outwards. This term is responsible for the mass loss in the wind. Next we derive the vertical momentum balance equation which is obtained from the z component of Eqn. (8).

$$2 \int_0^h \left[\bar{\rho} \bar{v}_r \frac{\partial \bar{v}_z}{\partial r} + \bar{\rho} \bar{v}_z \frac{\partial \bar{v}_z}{\partial z} + \bar{\rho} F_{Gz} + \frac{\partial \bar{P}}{\partial z} + \frac{\partial}{\partial z} \left(\frac{\bar{B}_\varphi^2 + \bar{B}_r^2}{8\pi} \right) - \frac{\bar{B}_r}{4\pi} \frac{\partial \bar{B}_z}{\partial r} \right] dz = 0, \quad (11)$$

where F_{Gz} is the vertical component of the gravitational force. Equation (11) is integrated from 0 to h due to the reflection symmetry of all the dynamical variables across the accretion-outflow coupled surface. Equation (11) contains the information of the outflow dynamics within the accretion-outflow region. The matter starts to accelerate vertically outwards from just above the equatorial plane of the accretion region. If there is no outflow, then $v_z = 0$, and if we neglect the magnetic pressure and magnetic stresses, Eqn. (11) reduces to the well known hydrostatic equilibrium condition in the disk, and the usual hydrostatic disk scale-height can be obtained.

(c) Divergence condition:

$$\int_{-h}^{+h} \left[\frac{1}{r} \frac{\partial}{\partial r} (r \bar{B}_r) + \frac{\partial \bar{B}_z}{\partial z} \right] dz = 0. \quad (12)$$

The divergence condition determines the symmetry property of magnetic field components. Whether the radial and the vertical component of the magnetic field will follow odd and even symmetry or vice-versa in the z direction, can be ascertained from the above equation.

(d) Magnetic induction:

The turbulent magnetic induction equation is derived from the mean field MHD theory (e.g., [31]). Following the usual procedure and neglecting the dynamo effect, the steady state induction equation in the tensorial form is given by

$$\epsilon_{ijk} \epsilon_{kmn} \frac{\partial}{\partial x_j} (\bar{v}_m \bar{B}_n) - \epsilon_{ijk} \frac{\partial}{\partial x_j} \left(\epsilon_{kmn} \nu_{ml}^{\mathcal{R}} \frac{\partial \bar{B}_n}{\partial x_l} \right) = 0, \quad (13)$$

where $\nu_{ml}^{\mathcal{R}}$ is the kinetic part of the turbulent viscosity. The above equation has been written in the most general form considering an anisotropic turbulence. Splitting Eqn. (13) in radial and azimuthal direction we obtain after vertical integration

$$\int_{-h}^{+h} \left[\frac{\partial}{\partial z} (\bar{v}_r \bar{B}_z - \bar{v}_z \bar{B}_r) + \frac{\partial}{\partial z} \left(\nu_{zz}^{\mathcal{R}} \frac{\partial \bar{B}_r}{\partial z} - \nu_{rr}^{\mathcal{R}} \frac{\partial \bar{B}_z}{\partial r} \right) \right] dz = 0. \quad (14)$$

and

$$\int_{-h}^{+h} \left[\frac{\partial}{\partial z} (\bar{v}_\varphi \bar{B}_z - \bar{v}_z \bar{B}_\varphi) - \frac{\partial}{\partial r} (\bar{v}_r \bar{B}_\varphi - \bar{v}_\varphi \bar{B}_r) + \frac{\partial}{\partial z} \left(\nu_{zz}^{\mathcal{R}} \frac{\partial \bar{B}_\varphi}{\partial z} \right) + \frac{\partial}{\partial r} \left(\nu_{rr}^{\mathcal{R}} \frac{\partial \bar{B}_\varphi}{\partial r} + \nu_{\varphi\varphi}^{\mathcal{R}} \frac{\bar{B}_\varphi}{r} \right) \right] dz = 0. \quad (15)$$

We do not show here the vertical component of the induction equation as it is similar to that of the radial equation, and contains the same information regarding the magnetic dynamics of the flow. Note that the turbulent diffusion in the induction equation arises only from the kinetic part of the turbulent stress tensor through the Reynolds stress. This is attributed to the mean field approximation, where we split the quantities in mean and turbulent part.

(e) Energy conservation:

The Poynting flux S_j is given by

$$S_j = \frac{c}{4\pi} \epsilon_{jlm} E_l B_m. \quad (16)$$

Using mean field MHD and the induction equation, and by discarding the microscopic resistivity, we write

$$\frac{\partial \bar{S}_j}{\partial x_j} = \frac{\bar{v}_j}{c} \epsilon_{jlm} \bar{B}_l \bar{J}_m + \frac{\bar{J}_j}{c} \epsilon_{jlm} \overline{v'_l B'_m} + \frac{\bar{v}_j}{c} \epsilon_{jlm} \overline{B'_l J'_m} + \frac{\bar{B}_j}{c} \epsilon_{jlm} \overline{J'_l v'_m}, \quad (17)$$

where J is the current density. In contrast to the other correlation terms, the last term in the right hand side of Eqn. (17) is not a first order correlation term, rather a second order or higher order correlation term [32]; we omit this term in our present study. Neglecting the kinetic dynamo effect, using Eqn. (17), the steady state energy conservation equation of a turbulent magnetic fluid in a tensorial form using mean field MHD is then given by

$$\frac{\partial}{\partial x_j} \left[\bar{\rho} \bar{v}_j \left(\frac{\bar{v}^2}{2} + \frac{8-3\beta}{2\beta} \frac{\bar{P}_g}{\bar{\rho}} + \varphi_G \right) - \bar{v}_i \overline{t_{ij}^{\mathcal{R}}} \right] + \frac{\bar{v}_j}{c} \epsilon_{jlm} \bar{B}_l \bar{J}_m + \frac{\bar{v}_j}{c} \epsilon_{jlm} \overline{B'_l J'_m} - \frac{1}{4\pi} \epsilon_{jlm} \nu_{lk}^{\mathcal{R}} \frac{\partial \bar{B}_m}{\partial x_k} \epsilon_{jlm} \frac{\partial \bar{B}_m}{\partial x_l} + \frac{\partial F_j^r}{\partial x_j} = 0, \quad (18)$$

where $\beta = \bar{P}_g / (\bar{P}_g + \bar{P}_r)$, the ratio of gas pressure to the total pressure in the accretion-outflow coupled region is assumed to be constant. \bar{P}_r is the radiation pressure in the gas-radiation mixture. The radiation field has been assumed to be locally isotropic. The ratio of specific heat of the fully ionized gas and radiation are taken as $\gamma_g = 5/3$

and $\gamma_r = 4/3$ respectively. The ‘effective ratio of specific heat’ Γ is related to β through $\Gamma = (8 - 3\beta)/(6 - 3\beta)$. In deriving Eqn. (18), we have neglected the turbulent thermal conductivity. The last term in the above equation represents the transport of radiative flux. Multiplying Eqn. (8) by \bar{v}_j and using the continuity equation, the vertically integrated energy budget for accretion-induced outflow is thus obtained below

$$\begin{aligned} \int_{-h}^{+h} \left[\frac{3}{2}(2 - \beta)\bar{\rho}\bar{v}_r\frac{\partial\bar{c}_s^2}{\partial r} - \bar{v}_r\bar{c}_s^2\frac{\partial\bar{\rho}}{\partial r} \right] dz + \int_{-h}^{+h} \left[\frac{3}{2}(2 - \beta)\bar{\rho}\bar{v}_z\frac{\partial\bar{c}_s^2}{\partial z} - \bar{v}_z\bar{c}_s^2\frac{\partial\bar{\rho}}{\partial z} \right] dz \\ = \int_{-h}^{+h} \left[\bar{\rho}\nu_{r\varphi}^{\mathcal{R}}\bar{s}_{r\varphi}^2 + \frac{1}{4\pi}\epsilon_{jlm}\nu_{lk}^{\mathcal{R}}\frac{\partial\bar{B}_m}{\partial x_k}\epsilon_{jlm}\frac{\partial\bar{B}_m}{\partial x_l} \right] dz - 2F^{r+}. \end{aligned} \quad (19)$$

Left hand side of the above equation is the signature of advection of energy flux in radial and vertical direction due to accretion and outflow respectively. First and the second term of the right hand side expresses the turbulent viscous heating due to $r\varphi$ component of the stress tensor and the turbulent Ohmic dissipation or Joule’s heat loss respectively in the accretion flow. Turbulent Ohmic dissipation symbolizes a resistive flow due to which constant annihilation of the magnetic flux occurs. The last term of the equation is the flux of radiation that is escaping from the accretion-outflow surface. Similar to that of the induction Eqn. (13), the turbulent diffusion in the energy equation also arises only through the Reynolds stress tensor

The net heat flux generated in the accretion flow is defined by

$$q^+ = \int_{-h}^{+h} \left(\bar{\rho}\nu_{r\varphi}^{\mathcal{R}}\bar{s}_{r\varphi}^2 + \frac{1}{4\pi}\epsilon_{jlm}\nu_{lk}^{\mathcal{R}}\frac{\partial\bar{B}_m}{\partial x_k}\epsilon_{jlm}\frac{\partial\bar{B}_m}{\partial x_l} \right) dz. \quad (20)$$

Defining f as a constant cooling factor scaled through a relation

$$q^+ - 2F^{r+} = (1 - f)q^+, \quad (21)$$

the final form of the heat flux equation is obtained by coupling Eqns. (19), (20) and (21). A constant f implies that the radiative heat loss from the accretion surface has a linear proportionality with the net heat flux generated in the system. Although f should vary radially, however, within a small inner accretion region where the accretion and outflow are coupled, this presumption is an acceptable approximation. The parameter f reflects the extent to which the accretion flow is advective. $f \rightarrow 1$ represents an accretion flow with efficient cooling or is radiatively efficient. At the other extremity, $f \rightarrow 0$ epitomize a strongly advective or advection dominated system which are radiatively inefficient.

Equations (7), (9), (10), (11), (12), (14), (15) and (19) exhibit the dynamical behavior of accretion-induced outflow in a resistive MHD paradigm in mean field approximation. In the next section, we explore a technique to solve these eight coupled partial differential equations using Eqns. (5), (20) and (21), rigorously.

III. POLYNOMIAL EXPANSION AND SOLUTION PROCEDURE

The equations describing the turbulent magneto-fluid in the last section are extremely complicated and it is beyond our scope to solve them numerically. The only procedure left in our hand is to explore some kind of approximate analytical method or quasi-analytical method to solve them. We follow a power law self-similar approach (see also NY94) with a polynomial expansion to solve the equations to obtain the class of solutions. For the present purpose we invoke a generalized n^{th} degree polynomial expansion of all the dynamical variables, where the flow variables are functions of both radial and vertical coordinate. We restrict ourselves in Newtonian paradigm as power law self-similar solutions are valid only in the limit of Newtonian approximation. The generalized Newtonian potential at any (r, z) in the accretion-outflow region is written in the form of power series

$$\varphi_G(r, z) = -GM(r^{-1} - \frac{1}{2}r^{-3}z^2 + \frac{3}{8}r^{-5}z^4 - \dots), \quad (22)$$

where M is the mass of the central object. The gravitational force in the radial and vertical direction is then written in the form of a polynomial expansion as shown below.

$$F_{Gr}(r, z) = GM \sum_{n=0}^{\infty} \binom{-3/2}{n} r^{-2-2n} z^{2n}. \quad (23)$$

$$F_{Gz}(r, z) = GM \sum_{n=0}^{\infty} \binom{-3/2}{n} r^{-3-2n} z^{2n+1}. \quad (24)$$

F_{Gr} and F_{Gz} have even and odd symmetry in z direction, respectively. We seek a polynomial expansion in the similar form for all dynamical variables, where the flow of matter in the accretion region is being considered to have reflection symmetry about the equatorial plane. All the hydrodynamical variables will have even symmetry except those directly related to F_{Gz} . The outflow velocity v_z will then have a odd symmetry in z direction. Consequently, the radial component of the magnetic field \bar{B}_r and the vertical component of the magnetic field B_z will have even and odd symmetry configuration, respectively, which is required from the divergence condition of the magnetic field. Odd symmetry configuration of magnetic field has been used previously on other occasions in context to outflows/jets from the accretion flows (e.g., [33,26]). The flow velocities, angular momentum and the density are then written in the following polynomial form

$$\begin{aligned} \bar{v}_r(r, z) &= \sum_{n=0}^{\infty} v_{r2n} r^{a-2n} z^{2n}, \bar{v}_\varphi(r, z) = \sum_{n=0}^{\infty} v_{\varphi 2n} r^{b-2n} z^{2n}, \\ \bar{\lambda}(r, z) &= \sum_{n=0}^{\infty} v_{\varphi 2n} r^{b-2n+1} z^{2n}, \bar{v}_z(r, z) = \sum_{n=0}^{\infty} v_{z(2n+1)} r^{c-2n} z^{2n+1}, \\ \bar{c}_s(r, z) &= \sum_{n=0}^{\infty} c_{s2n} r^{d-2n} z^{2n}, \bar{\rho}(r, z) = \sum_{n=0}^{\infty} \rho_{2n} r^{e-2n} z^{2n}. \end{aligned} \quad (25)$$

Similarly, the components of the magnetic field can be expanded as

$$\bar{B}_r(r, z) = \sum_{n=0}^{\infty} B_{r2n} r^{i-2n} z^{2n}, \bar{B}_\varphi(r, z) = \sum_{n=0}^{\infty} B_{\varphi 2n} r^{j-2n} z^{2n}, \bar{B}_z(r, z) = \sum_{n=0}^{\infty} B_{z(2n+1)} r^{k-2n} z^{2n+1}, \quad (26)$$

where, v_{r2n} , $v_{\varphi 2n}$, $v_{z(2n+1)}$, c_{s2n} , ρ_{2n} , B_{r2n} , $B_{\varphi 2n}$, $B_{z(2n+1)}$ are the dimensionless coefficients which will be evaluated from the MHD conservation equations.

We determine the exponents a, b, c, d, e, i, j, k by self comparison of various terms in the model equations. Substituting the solutions from Eqns. (25) and (26) in the MHD conservation equations and comparing the exponents of r and z , we obtain $a = -1/2$, $b = -1/2$, $c = -3/2$, $d = -1/2$, $e = -3/2$, $i = -5/4$, $j = -5/4$, $k = -9/4$.

Using the above value of exponents and using the polynomials in Eqns. (25) and (26), Eqns. (9), (10), (11), (12), (14), (15) and (19) can be expanded in the power of aspect ratio (h/r). Using a simple technique given by the form

$$\sum_{n=0}^{\infty} u_n x^n \sum_{n=0}^{\infty} v_n x^n \sum_{n=0}^{\infty} w_n x^n = \sum_{n=0}^{\infty} x^n \sum_{m=0}^{\infty} \sum_{l=0}^{\infty} u_{n-m} v_{m-l} w_l, \quad (27)$$

the above polynomial equations then can be written in a generic form as

$$A_0 \left(\frac{h}{r}\right)^0 + A_1 \left(\frac{h}{r}\right)^2 + A_2 \left(\frac{h}{r}\right)^4 + \dots = 0, \quad (28)$$

where, A_0, A_1, A_2, \dots are zeroth order, first order, second order and higher order coefficients which are nonlinear functions of v_{r2n} , $v_{\varphi 2n}$, $v_{z(2n+1)}$, c_{s2n} , ρ_{2n} , B_{r2n} , $B_{\varphi 2n}$, $B_{z(2n+1)}$ corresponding to $n = 0, n = 1, n = 2, \dots$, respectively. Equation (28) is a linear combination in powers of h/r which are linearly independent.

If we neglect all the terms of the order $\geq (h/r)^2$, and only keep the zeroth order term, the generic Eqn. (28) after neglecting the magnetic field contribution will reduce to algebraic equations in NY94. To exemplify, in the appendix, we have shown the polynomial expansion of the integro-differential mass transfer Eqn. (7) and the radial momentum balance Eqn. (9) explicitly. Even if the accretion flow has considerable thickness, h in general would always be less than r . Further, magnetic stresses will compress or squeeze the accretion region. Considering the expression in Eqn. (28) up to the term $(h/r)^2$ would then be a reasonable approximation. Restricting the expansion up to $(h/r)^2$ corresponding to $n = 1$ and neglecting the terms with orders $\geq (h/r)^4$ in the generic expression (28), we equate A_0 and A_1 to zero, respectively. Extending this to MHD conservation equations and assuming isotropic turbulence, after rigorous algebra, we will then have fifteen independent non-linear algebraic equations with sixteen unknown coefficients consisting of zeroth and first order only, which are shown below.

Equation (7) renders

$$\rho_0(v_{r0} - v_{z1})t + [\rho_0(v_{r2} - v_{z3}) + \rho_2(v_{r0} - v_{z1})] \frac{t^3}{3} = -\frac{\dot{M}}{4\pi}. \quad (29)$$

Equation (12) renders

$$B_{z1} = \frac{B_{r0}}{4}, \quad (30)$$

$$B_{z3} = \frac{3}{4}B_{r2}. \quad (31)$$

Equation (9) renders

$$-\frac{1}{2}v_{r0}^2 - v_{\varphi0}^2 + GM - \frac{5}{2}c_{s0}^2 - \frac{1}{16\pi} \frac{B_{\varphi0}^2}{\rho_0} = 0, \quad (32)$$

$$\begin{aligned} -\frac{1}{2}\rho_2 v_{r0}^2 - 3\rho_0 v_{r0} v_{r2} - \rho_2 v_{\varphi0}^2 - 2\rho_0 v_{\varphi0} v_{\varphi2} + 2\rho_0 v_{z1} v_{r2} + GM(\rho_2 - \frac{3}{2}\rho_0) - \frac{9}{2}(\rho_2 c_{s0}^2 + 2\rho_0 c_{s0} c_{s2}) \\ + \frac{1}{4\pi}(-\frac{5}{2}B_{\varphi0} B_{\varphi2} - \frac{9}{4}B_{z1}^2 - 2B_{z1} B_{r2}) = 0. \end{aligned} \quad (33)$$

Equation (10) renders

$$\frac{1}{2}v_{r0} v_{\varphi0} + \frac{3}{4}\alpha_{r\varphi} t v_{\varphi0} c_{s0} + \frac{1}{16\pi} \frac{B_{r0} B_{\varphi0}}{\rho_0} = 0, \quad (34)$$

$$\begin{aligned} \frac{1}{2}(\rho_2 v_{r0} v_{\varphi0} + \rho_0 v_{\varphi0} v_{r2}) - \frac{3}{2}\rho_0 v_{r0} v_{\varphi2} + 2\rho_0 v_{z1} v_{\varphi2} + \frac{1}{2}\alpha_{r\varphi} t \left(\frac{3}{2}\rho_2 c_{s0} v_{\varphi0} + \frac{3}{2}\rho_0 c_{s2} v_{\varphi0} + \frac{7}{2}\rho_0 c_{s0} v_{\varphi2} \right) \\ + \frac{1}{16\pi}(B_{\varphi0} B_{r2} + 7B_{r0} B_{\varphi0}) = 0. \end{aligned} \quad (35)$$

Equation (11) renders

$$-\frac{3}{2}\rho_0 v_{r0} v_{z1} + \rho_0 v_{z1}^2 + \rho_0 GM + 2(\rho_2 c_{s0}^2 + 2\rho_2 c_{s0} c_{s2}) + \frac{1}{4\pi}(2B_{r0} B_{r2} + 2B_{\varphi0} B_{\varphi2} + \frac{9}{4}B_{r0} B_{z1}) = 0, \quad (36)$$

$$\begin{aligned} -\frac{3}{2}\rho_2 v_{r0} v_{z1} - \frac{3}{2}\rho_0 v_{r2} v_{z1} - \frac{7}{2}\rho_0 v_{r0} v_{z3} + \rho_2 v_{z1}^2 + 4\rho_0 v_{z1} v_{z3} + GM(\rho_2 - \frac{3}{2}\rho_0) + 4(\rho_2 c_{s0} c_{s2} + \rho_0 c_{s2}^2) \\ + \frac{1}{8\pi}(4B_{r2}^2 + 4B_{\varphi2}^2) - \frac{1}{4\pi} \left(-\frac{9}{4}B_{r2} B_{z1} - \frac{17}{4}B_{r0} B_{z3} \right) = 0. \end{aligned} \quad (37)$$

Equation (14) renders

$$(v_{r0} B_{z1} - v_{z1} B_{r0}) + \alpha_{r\varphi}^{\mathcal{R}} t \left(2c_{s0} B_{r2} + \frac{9}{4}c_{s0} B_{z1} \right) = 0. \quad (38)$$

$$(v_{r2} B_{z1} + v_{r0} B_{z3}) - (v_{z3} B_{r0} + v_{z1} B_{r2}) + \alpha_{r\varphi}^{\mathcal{R}} t \left(2c_{s2} B_{r2} + \frac{9}{4}c_{s2} B_{z1} + \frac{17}{4}c_{s0} B_{z3} \right) = 0. \quad (39)$$

Equation (15) renders

$$(v_{\varphi0} B_{z1} - v_{z1} B_{\varphi0}) + \frac{7}{4}(v_{r0} B_{\varphi0} - v_{\varphi0} B_{r0}) + \alpha_{r\varphi}^{\mathcal{R}} t \left(2c_{s0} B_{\varphi2} + \frac{7}{16}c_{s0} B_{\varphi0} \right) = 0, \quad (40)$$

$$3(v_{\varphi 0} B_{z3} - v_{\varphi 2} B_{z1}) - 3(v_{z3} B_{\varphi 0} - v_{z1} B_{\varphi 2}) + \frac{7}{4}[(v_{r0} B_{\varphi 2} + v_{r2} B_{\varphi 0}) - (v_{\varphi 2} B_{r0} + v_{\varphi 0} B_{r2})] \\ + \alpha_{r\varphi}^{\mathcal{R}} t \left[6 c_{s2} B_{\varphi 2} + \frac{15}{16}(c_{s2} B_{\varphi 0} + 9 c_{s0} B_{\varphi 2}) \right] = 0. \quad (41)$$

Equation (19) using Eqns. (20) and (21) renders

$$\frac{3}{2}(\beta - 1) v_{r0} c_{s0} = (1 - f) \alpha_{r\varphi}^{\mathcal{R}} t \left(\frac{9}{4} v_{\varphi 0}^2 + \frac{1}{16} \frac{B_{\varphi 0}^2}{4\pi \rho_0} \right), \quad (42)$$

$$\frac{3}{2}(\beta - 1) \rho_0 v_{r2} c_{s0}^2 + (9\beta - 15) \rho_0 v_{r0} c_{s0} c_{s2} + \frac{1+3\beta}{2} \rho_2 v_{r0} c_{s0}^2 + 6(2 - \beta) \rho_0 v_{z1} c_{s0} c_{s2} - 2\rho_2 v_{z1} c_{s0}^2 \\ = (1 - f) \alpha_{r\varphi}^{\mathcal{R}} t \left[\left(\frac{9}{4} \rho_2 c_{s0} v_{\varphi 0}^2 + \frac{9}{4} \rho_0 c_{s2} v_{\varphi 0}^2 + \frac{21}{2} \rho_0 c_{s0} v_{\varphi 0} v_{\varphi 2} \right) + \frac{1}{4\pi} \left(4 c_{s0} B_{\varphi 2}^2 + 4 c_{s0} B_{r2}^2 + \frac{81}{16} c_{s0} B_{z1}^2 + 9 c_{s0} B_{r2} B_{z1} \right. \right. \\ \left. \left. + \frac{1}{16} c_{s2} B_{\varphi 0}^2 + \frac{9}{8} c_{s0} B_{\varphi 0} B_{\varphi 2} \right) \right]. \quad (43)$$

In the above equations $t = h(r)/r$. Using Eqns. (29), (30), (31), (33), (34), (35), (36), (38), (39), (40), (42), and after very complicated and tedious algebra, we systematically determine the value of all the first order coefficients in terms of zeroth order coefficients of hydrodynamic variables. Substituting them in Eqns. (32), (37), (41) and (43), we successfully reduce fifteen equations to four nonlinear algebraic equations comprising of zeroth order coefficients $v_{z1}, v_{\varphi 0}, B_{r0}$ and $B_{\varphi 0}$ only. We then solve the above four nonlinear equations through an iterative Newton Raphson method for appropriate initial guess. In these way we can obtain the values of zeroth and first order coefficients of the corresponding dynamical variables. The value of the coefficients are scaled by putting $G = M = 1$, and \dot{M} in units of \dot{M}_{Edd} .

In the next section, we evaluate them for appropriate choice of parameters \dot{M} , β and f .

IV. EVALUATION OF THE COEFFICIENTS

In §I we have analyzed the necessity to have a sub-Keplerian advective accretion regime to eject strong outflows and jets from the accretion region in the vicinity of the BHs. The corresponding accretion regime can be possibly envisaged if the mass accretion rate or net mass flow rate is considerably sub-Eddington ($\dot{M} \lesssim 10^{-2} \dot{M}_{\text{Edd}}$). The ratio of gas to the total pressure β and the radiative cooling factor f directly depends on \dot{M} . Looking meticulously into the equations from (29 – 43), we notice that the continuity equation is written in the integral form through Eqn. (29), unlike the other hydrodynamical equations. This is being deliberately done to preserve the information of \dot{M} in the flow, as \dot{M} is the most fundamental parameter which determines the nature of the BH accretion paradigm. However, this constraints the number of dynamical equations. For our case, we have sixteen unknown coefficients but fifteen number of equations. To resolve this, we proceed in the following way.

\dot{M} carries the information of the density of the flow which means that if \dot{M} is known, in principle, density too is known. Equation (29) reveals that the density in the accretion-outflow region is a function of two unknown coefficients ρ_0 and ρ_2 . ρ_0 is the signature of inflow whereas ρ_2 is that of the outflow. If the outflow is discarded, ρ_2 loses its significance and \dot{M} then becomes the usual mass accretion rate from where ρ_0 can be easily calculated. If r_j represents the outer radial boundary of the accretion-outflow coupled region, then at $r \geq r_j$ the net mass flow \dot{M} is equivalent to the mass accretion rate of the flow. At $r \geq r_j$, density of the accretion flow is just a function of ρ_0 , which is then given by (also see [5])

$$\rho_0 = \frac{\left[5 + 2 \frac{1-\beta}{1-f} \frac{\alpha_{r\varphi}}{\alpha_{r\varphi}^{\mathcal{R}}} \right]^{3/2}}{12\pi\sqrt{2}} \frac{\dot{M}}{\alpha_{r\varphi}}. \quad (44)$$

$\alpha_{r\varphi}^{\mathcal{R}}$ arises due to mean field approximation. Note that, the value of ρ_0 computed in Eqn. (44) is not exactly the same as that of ρ_0 in Eqn. (29), where it is coupled to ρ_2 . However, we presume that the density in the accretion flow does not change abruptly due to emanation of the outflow and jet, as only a small fraction of matter is ejected

out through the outflow. With this presumption, we calculate ρ_0 in Eqn. (29) using Eqn. (44), and supply its value to the rest of other nonlinear equations for further computation.

In the usual accretion flow, when there is no net vertical flux, the vertical height of the accretion geometry is calculated from the hydrostatic pressure balance, assuming the pressure and density at the outer accretion surface to be zero. However, this physical condition cease to exist when the outflow is incorporated in the system, and the scale-height of the coupled accretion-induced outflow region becomes difficult to ascertain. In these circumstances accretion-outflow coupled surface can be treated as a photospheric height, delineating between the accretion-outflow surface and the transition region leading to the outflow decoupling from the inflow. We treat $t = h(r)/r$ as a parameter to get physical plausible solutions.

Pessah, Chan and Psaltis [34] had shown that during the exponential growth of magnetorotational instability at saturation, the ratio of Maxwell stress to Reynolds stress becomes

$$\frac{\overline{t_{r\varphi}^{\mathcal{M}}}}{\overline{t_{r\varphi}^{\mathcal{R}}}} = \frac{4-q}{q}, \quad (45)$$

where $3/2 \leq q < 2$. q is related to the angular velocity through the relation $\Omega \sim r^{-q}$. $q = 3/2$ signifies an Keplerian flow whereas $q > 3/2$ implies a sub-Keplerian or an advective accretion flow. Thus for a strongly advective flow $q \gg 3/2$. We use the relation given in Eqn. (45) to determine the value of $\alpha_{r\varphi}^{\mathcal{R}}$ used in our equations, which is then related to $\alpha_{r\varphi}$ as

$$\frac{\alpha_{r\varphi}^{\mathcal{R}}}{\alpha_{r\varphi}} = \frac{q}{4}. \quad (46)$$

The qualitative feature of the dynamical coefficients for an accretion-induced outflow which are physically plausible should satisfy the following properties of the flow variables; $\bar{v}_r \rightarrow$ negative, $\bar{v}_z \rightarrow$ positive, $\bar{B}_{\varphi 0} \rightarrow$ negative. All the other variables should have a positive value. The positivity of \bar{B}_r and \bar{B}_z is related to the open magnetic field lines threading the accretion flow, across which the accreting matter diffuses, and then gets accelerated outwards along the poloidal field lines by extracting the angular momentum from the flow. The term $-r^2(\bar{B}_{\varphi}\bar{B}_z)_h$ [last term in Eqn. (10)], which is a magnetic torque on the accretion flow is attributed to the transport of angular momentum from the $h(r)$ surfaces of the accretion-outflow region outwards. This term should be positive in order to launch a jet, which removes angular momentum from the flow and decouples from the accretion region. This premise makes a obvious choice for \bar{B}_{φ} to have a negative value. It should be reminded that the negative value of many quantities do not necessarily mean that their magnitude is negative, but it represents the direction of their flow.

Next we compute the value of the coefficients of all dynamical variables for three relevant choices of \dot{M} with appropriate values of β and f , conducive to form outflows and jets.

A. Case 1. For $\dot{M} = 10^{-4} \dot{M}_{\text{Edd}}$

The particular choice of \dot{M} corresponds to RIAF, which is linked observationally to low-hard state of BHXRBs and LERGs/LLAGNs. This type of flow is significantly gas pressure dominated, and strongly advective. The flow is considerably geometrically thick, optically thin and radiatively inefficient. We choose appropriate values of β and f corresponding to this \dot{M} to get physical plausible solutions. As this flow is highly sub-Keplerian and strongly advective, an appropriate choice of value of $q \sim 1.9$ has been taken. In tables 1.1, 1.2 and 1.3, we present the computed values of the dynamical coefficients for $\beta = 0.95$, $f = 0.1$ with suitable choices of α and t . For $\beta \sim 0.95$, Γ is ~ 1.635 . It is interestingly found that for $q \ll 1.9$ and in the range of $1.9 \ll q < 2$, we never found any physically valid solutions. However, for much stronger advective paradigm ($\dot{M} \ll 10^{-4} \dot{M}_{\text{Edd}}$), one would still obtain physically correct solutions for $1.9 \ll q < 2$.

We will analyze the family of analytical solutions later, however, we note that the values of the coefficients are in conformity with desired physically valid solutions (mentioned earlier). We notice that they are obtained only at high α ($\gtrsim 0.3$) and at a reduced vertical scale-height ($t \sim 0.1$) of the accretion-outflow coupled region. Although t is small, it corresponds to a geometrically thick accretion flow ($t \gtrsim 0.1$, t measures the degree of flow thickness). We have elucidated the necessity of a geometrically thick accretion flow to eject outflow and jet in previous paragraphs. However, corresponding to $\alpha \sim 0.3$, we never found any physically acceptable solution for $t > 0.1$. For higher $\alpha \sim 0.5$, however, we obtain a solution at a maximum value of $t \sim 0.2$. This infers that with the increase of α , the plausible physical solutions can be obtained with a thicker accretion geometry. Nevertheless, very high α (> 0.5) accretion flow might not be realistic in nature, and hence we restrict our study to a maximum plausible value of $\alpha \sim 0.5$.

Table 1.1

$$\dot{M} = 10^{-4} \dot{M}_{\text{Edd}}, \beta = 0.95, f = 0.1, \alpha = 0.3, t = 0.1, q = 1.9.$$

| ρ_0 | v_{r0} | $v_{\varphi 0}$ | v_{z1} | c_{s0} | B_{r0} | $B_{\varphi 0}$ | B_{z1} |
|------------|----------|-----------------|----------|----------|----------|-----------------|----------|
| 7.4864e-5 | -0.0899 | 0.3692 | 0.7069 | 0.5867 | 0.0036 | -0.0050 | 1.3e-3 |
| ρ_2 | v_{r2} | $v_{\varphi 2}$ | v_{z3} | c_{s2} | B_{r2} | $B_{\varphi 2}$ | B_{z3} |
| -3.4889e-4 | -0.2421 | 0.3471 | -33.1161 | -0.3551 | 0.0523 | -0.2176 | 0.0793 |

Table 1.2

$$\dot{M} = 10^{-4} \dot{M}_{\text{Edd}}, \beta = 0.95, f = 0.1, \alpha = 0.5, t = 0.1, q = 1.9.$$

| ρ_0 | v_{r0} | $v_{\varphi 0}$ | v_{z1} | c_{s0} | B_{r0} | $B_{\varphi 0}$ | B_{z1} |
|------------|----------|-----------------|----------|----------|----------|-----------------|----------|
| 4.4918e-5 | -0.1494 | 0.3694 | 0.3859 | 0.5891 | 0.0051 | -0.0041 | 4.25e-3 |
| ρ_2 | v_{r2} | $v_{\varphi 2}$ | v_{z3} | c_{s2} | B_{r2} | $B_{\varphi 2}$ | B_{z3} |
| -1.1174e-4 | -0.0925 | 0.3211 | -7.0486 | -0.2300 | 0.0257 | -0.0603 | 0.0193 |

Obtaining physically valid solutions of an accretion-induced outflow at a reduced geometrical thickness (scale-height) of the accretion region, as compared to a non-magnetized accretion flow (without outflow) like ADAFs for a similar accretion paradigm, is owing to the fact, that the magnetic stresses in the flow has a tendency to squeeze or compress the region by acting oppositely to thermal pressure gradient, consequently reducing the scale-height of the accretion region. This squeezing effect has been discussed by several other authors (e.g., [25,30]) in context to magnetized accretion flow. This can be noticed from the vertical momentum balance equation (Eqn. 11). As we intend to see the effect of magnetic field on the geometrical thickness of the accretion region, for simplicity we ignore the outflow in (Eqn. 11). Further, we found that with the increase in z , the magnitude of all components of the magnetic field increases, however the density and the thermal pressure decreases with increase in z . As we ignore the outflow, for simplicity of our calculation, we consider density and thermal pressure at accretion flow scale-height (h) to be negligible as compared to their equatorial values; this will not alter the qualitative nature of our argument. Expanding the terms in (Eqn. 11), and restricting up to h^2/r^2 , (Eqn. 11) will reduce to the magnetohydrostatic equilibrium equation, given by

$$\bar{\rho}_{\text{eq}} \frac{h^2}{r^3} \sim \bar{P}_{\text{eq}} - \frac{1}{8\pi} r^{-5/4} \left(B_{\varphi 0} B_{\varphi 2} + B_{r0} B_{r2} + \frac{9}{4} B_{r0} B_{z1} \right) \frac{h^2}{r^2}, \quad (47)$$

where, $\bar{\rho}_{\text{eq}}$ and \bar{P}_{eq} are the density and thermal pressure at equatorial plane. The scale-height of the accretion flow would then approximately be given by

$$h \sim \sqrt{\frac{c_s^2 r^3}{1 + \frac{1}{8\pi\rho_0} (B_{\varphi 0} B_{\varphi 2} + B_{r0} B_{r2} + \frac{9}{4} B_{r0} B_{z1})}}. \quad (48)$$

If we neglect the magnetic components, Eqn. (47) is then the usual hydrostatic scale-height of the accretion flow. Due to the presence of magnetic field, the scale-height is now approximately reduced by a factor $\sqrt{1 + \frac{1}{8\pi\rho_0} (B_{\varphi 0} B_{\varphi 2} + B_{r0} B_{r2} + \frac{9}{4} B_{r0} B_{z1})}$.

Table 1.3

$$\dot{M} = 10^{-4} \dot{M}_{\text{Edd}}, \beta = 0.95, f = 0.1, \alpha = 0.5, t = 0.2, q = 1.9.$$

| ρ_0 | v_{r0} | $v_{\varphi 0}$ | v_{z1} | c_{s0} | B_{r0} | $B_{\varphi 0}$ | B_{z1} |
|------------|----------|-----------------|----------|----------|----------|-----------------|----------|
| 4.4918e-5 | -0.2876 | 0.3636 | 0.6211 | 0.5977 | 0.0149 | -0.0061 | 5.2e-3 |
| ρ_2 | v_{r2} | $v_{\varphi 2}$ | v_{z3} | c_{s2} | B_{r2} | $B_{\varphi 2}$ | B_{z3} |
| -2.1111e-4 | -0.7225 | 0.6940 | -9.7460 | -0.3859 | 0.0598 | -0.0724 | 0.0448 |

Table 2.1

$$\dot{M} = 10^{-3} \dot{M}_{\text{Edd}}, \beta = 0.9, f = 0.1, \alpha = 0.3, t = 0.1, q = 1.85.$$

| ρ_0 | v_{r0} | $v_{\varphi 0}$ | v_{z1} | c_{s0} | B_{r0} | $B_{\varphi 0}$ | B_{z1} |
|-----------|----------|-----------------|----------|----------|----------|-----------------|----------|
| 8.0216e-4 | -0.0900 | 0.5100 | 0.7370 | 0.5430 | 0.0028 | -0.0160 | 7e-4 |
| ρ_2 | v_{r2} | $v_{\varphi 2}$ | v_{z3} | c_{s2} | B_{r2} | $B_{\varphi 2}$ | B_{z3} |
| -4.7e-3 | -0.1960 | 0.2462 | -39.9113 | -0.3761 | 0.1411 | -0.8040 | 0.1058 |

Table 2.2

$$\dot{M} = 10^{-3} \dot{M}_{\text{Edd}}, \beta = 0.9, f = 0.1, \alpha = 0.5, t = 0.1, q = 1.85.$$

| ρ_0 | v_{r0} | $v_{\varphi 0}$ | v_{z1} | c_{s0} | B_{r0} | $B_{\varphi 0}$ | B_{z1} |
|----------|----------|-----------------|----------|----------|----------|-----------------|----------|
| 4.813e-4 | -0.1498 | 0.5106 | 0.4168 | 0.5451 | 0.0040 | -0.0136 | 1e-3 |
| ρ_2 | v_{r2} | $v_{\varphi 2}$ | v_{z3} | c_{s2} | B_{r2} | $B_{\varphi 2}$ | B_{z3} |
| -1.5e-3 | -0.0939 | 0.2377 | -9.0662 | -0.2749 | 0.0721 | -0.2418 | 0.0541 |

As the region becomes more compressed, the thermal content of the gas increases and the excess thermal pressure gradient will help in lifting the plasma vertically outwards.

B. Case 2. For $\dot{M} = 10^{-3} \dot{M}_{\text{Edd}}$

The accretion paradigm corresponding to this \dot{M} resembles that in case 1. We choose similar values of β , f , q and t to study the feature of accretion-outflow coupled dynamics. We consider two values of β , $\beta = 0.95$ and 0.9 corresponding to $q = 1.9$ and 1.85 respectively, keeping the cooling factor f same. This slightly less q for $\beta = 0.9$ is ascribed to the fact that with the decrease in β , the content of the gas pressure in the system decreases, which makes the flow to be less sub-Keplerian. Other values of α and t are same as in §IV(A). We do not show the values of the coefficients for $\beta \sim 0.95$, $q = 1.9$ as they are very similar to that of the scenario for $\dot{M} = 10^{-4} \dot{M}_{\text{Edd}}$, however, only present the values of the coefficients for $\beta \sim 0.9$, $q = 1.85$ in tables 2.1, 2.2, 2.3. The ‘effective ratio of specific heat’ Γ , corresponding to $\beta \sim 0.9$ is ~ 1.61 . Resembling the scenario corresponding to $\dot{M} = 10^{-4} \dot{M}_{\text{Edd}}$, here too, we get solutions only at high α and at a reduced t , the reason being argued in the previous subsection.

C. Case 3. For $\dot{M} = 10^{-2} \dot{M}_{\text{Edd}}$

The earlier values of \dot{M} in the previous subsections correspond to RIAF. Nonetheless, moderately advective accretion paradigm may also be susceptible to eject outflows and jets. These accretion flows which are less advective as compared to RIAFs, will have lesser gas pressure content and higher cooling efficiency, and are less geometrically thick and are centrifugally more dominating. They have a moderate optical depth. This accretion paradigm can be presumably envisaged with $10^{-3} \dot{M}_{\text{Edd}} \ll \dot{M} \lesssim 10^{-2} \dot{M}_{\text{Edd}}$; for our analysis, here, we choose $\dot{M} \sim 10^{-2} \dot{M}_{\text{Edd}}$.

We choose appropriate values of β and f corresponding to this \dot{M} to get physical plausible solutions. As this flow is sub-Keplerian and advective, q should be greater than 1.5, but considerably less than in flows illustrated in previous subsections. We choose the value of $q \sim 1.75$. For $1.5 < q \ll 1.75$ and for $1.75 \ll q < 1.85$, we never found any

Table 2.3

$$\dot{M} = 10^{-3} \dot{M}_{\text{Edd}}, \beta = 0.9, f = 0.1, \alpha = 0.5, t = 0.2, q = 1.85.$$

| ρ_0 | v_{r0} | $v_{\varphi 0}$ | v_{z1} | c_{s0} | B_{r0} | $B_{\varphi 0}$ | B_{z1} |
|----------|----------|-----------------|----------|----------|----------|-----------------|----------|
| 4.813e-4 | -0.2948 | 0.5090 | 0.6330 | 0.5533 | 0.0127 | -0.0216 | 3.2e-3 |
| ρ_2 | v_{r2} | $v_{\varphi 2}$ | v_{z3} | c_{s2} | B_{r2} | $B_{\varphi 2}$ | B_{z3} |
| -2.8e-3 | -0.5535 | 0.5914 | -11.3549 | -0.4235 | 0.1753 | -0.2907 | 0.1315 |

Table 3.1

$$\dot{M} = 10^{-2} \dot{M}_{\text{Edd}}, \beta = 2/3, f = 0.5, \alpha = 0.3, t = 0.05, q = 1.75.$$

| ρ_0 | v_{r0} | $v_{\varphi 0}$ | v_{z1} | c_{s0} | B_{r0} | $B_{\varphi 0}$ | B_{z1} |
|----------|----------|-----------------|-----------|----------|----------|-----------------|----------|
| 0.0143 | -0.0509 | 0.9211 | 0.6728 | 0.2462 | 0.0017 | -0.0293 | 4.25e-4 |
| ρ_2 | v_{r2} | $v_{\varphi 2}$ | v_{z3} | c_{s2} | B_{r2} | $B_{\varphi 2}$ | B_{z3} |
| -0.3132 | -0.4994 | -0.0714 | -152.2853 | -0.8796 | 0.3606 | -6.1736 | 0.2704 |

Table 3.2

$$\dot{M} = 10^{-2} \dot{M}_{\text{Edd}}, \beta = 2/3, f = 0.5, \alpha = 0.5, t = 0.05, q = 1.75.$$

| ρ_0 | v_{r0} | $v_{\varphi 0}$ | v_{z1} | c_{s0} | B_{r0} | $B_{\varphi 0}$ | B_{z1} |
|----------|----------|-----------------|----------|----------|----------|-----------------|----------|
| 0.0086 | -0.0847 | 0.9218 | 0.4130 | 0.2468 | 0.0024 | -0.0253 | 6e-4 |
| ρ_2 | v_{r2} | $v_{\varphi 2}$ | v_{z3} | c_{s2} | B_{r2} | $B_{\varphi 2}$ | B_{z3} |
| -0.1119 | -0.4971 | -0.1303 | -38.7978 | -0.5916 | 0.1930 | -2.0099 | 0.1447 |

physically valid solutions with $\dot{M} \sim 10^{-2} \dot{M}_{\text{Edd}}$. However, in the stated range one may still obtain valid solutions, either for $\dot{M} \gg 10^{-2} \dot{M}_{\text{Edd}}$ or for $\dot{M} \ll 10^{-2} \dot{M}_{\text{Edd}}$, respectively.

We evaluate the value of the dynamical coefficients for appropriate choice of $\beta \sim 2/3$ with $f = 0.4, 0.5$ corresponding to $\dot{M} \sim 10^{-2} \dot{M}_{\text{Edd}}$. The values of α are same as before. We found that for $f > 0.5$ or $\beta \lesssim 0.6$, the flow becomes near Keplerian ($v_{\varphi 0} \sim 1$) and we get the physical solutions only at $t < 0.05$. Such a flow is not favourable for ejection of outflow as reasoned earlier. Hence we restrict our study to a maximum value of $f = 0.5$ corresponding to $\beta \sim 2/3$. Corresponding Γ for $\beta \sim 2/3$ is 1.5. In tables 3.1, 3.2, 3.3, we present them for $f = 0.5$ for appropriate values of t .

For an easy comparison we furnish the values of $v_{\varphi 2}$ corresponding to $f = 0.4$ for $\dot{M} \sim 10^{-2} \dot{M}_{\text{Edd}}$, with appropriate α and t in Table 4, whose importance we will notice as we proceed.

We found that we do not obtain any solution for $t > 0.05$ with $\alpha = 0.3$, and $t > 0.1$ for $\alpha = 0.5$. The reason of physical solutions of accretion-induced outflow at a reduced scale-height has been stated in §IV(A). However, obtaining physically valid solutions with $\dot{M} \sim 10^{-2} \dot{M}_{\text{Edd}}$ at a slightly reduced scale-height as compared to that obtained with $\dot{M} \lesssim 10^{-3} \dot{M}_{\text{Edd}}$ is consistent with the fact, that as $\dot{M} > 10^{-3} \dot{M}_{\text{Edd}}$, the accretion flow tends to become more rotationally dominated with diminishing degree of advection.

If we compare the value of the dynamical coefficients for $\dot{M} \lesssim 10^{-3} \dot{M}_{\text{Edd}}$ and $\dot{M} \sim 10^{-2} \dot{M}_{\text{Edd}}$, we found a fundamental difference in the dynamical nature of \bar{v}_{φ} . For $\dot{M} \lesssim 10^{-3} \dot{M}_{\text{Edd}}$, the value of the coefficient $v_{\varphi 2}$ is always positive. On the contrary, the value of $v_{\varphi 2}$ is negative for $\dot{M} \sim 10^{-2} \dot{M}_{\text{Edd}}$. Negative value of $v_{\varphi 2}$ implies that \bar{v}_{φ} decreases in z in the coupled accretion outflow region for $\dot{M} \sim 10^{-2} \dot{M}_{\text{Edd}}$. To verify this anomaly, we evaluated $v_{\varphi 2}$ for lower β and higher f , and vice-versa. It is revealing that for $f > 0.3$ and $\beta < 0.75$, we always obtain a negative $v_{\varphi 2}$ with $\alpha \sim 0.5$. $v_{\varphi 2} = 0.0162$ corresponding to $f = 0.3, \beta = 0.75$. With $\alpha \sim 0.3$ the negative values of $v_{\varphi 2}$ are obtained for $f \gtrsim 0.4$ and $\beta < 0.7$. The corresponding value of $v_{\varphi 2} = 0.0275$ for $f = 0.4$ and $\beta = 0.7$. To reassure ourselves we computed $v_{\varphi 2}$ for $\dot{M} \sim 10^{-1} \dot{M}_{\text{Edd}}$, and we arrive at a similar result. The above consistent findings convey that for strong gas pressure and advection dominated flows (RIAFs), \bar{v}_{φ} do not decrease in z within the accretion-outflow coupled region. On the contrary, for flows with lesser content of gas and higher cooling efficiency, which are less advective and centrifugally more dominating, \bar{v}_{φ} decreases in z within the coupled accretion-induced outflow region. We comment on this apparent dichotomy in §V. We also found that with a moderate decrease in α from 0.5 to 0.3,

Table 3.3

$$\dot{M} = 10^{-2} \dot{M}_{\text{Edd}}, \beta = 2/3, f = 0.5, \alpha = 0.5, t = 0.1, q = 1.75.$$

| ρ_0 | v_{r0} | $v_{\varphi 0}$ | v_{z1} | c_{s0} | B_{r0} | $B_{\varphi 0}$ | B_{z1} |
|----------|----------|-----------------|----------|----------|----------|-----------------|----------|
| 0.0086 | -0.1689 | 0.9244 | 0.6179 | 0.2492 | 0.0084 | -0.0441 | 2.1e-3 |
| ρ_2 | v_{r2} | $v_{\varphi 2}$ | v_{z3} | c_{s2} | B_{r2} | $B_{\varphi 2}$ | B_{z3} |
| -0.1931 | -1.1612 | -0.3876 | -46.8950 | -0.9662 | 0.5086 | -2.6172 | 0.3815 |

Table 4

| $\beta = 2/3, f = 0.4$ | | |
|------------------------|------|-----------------|
| α | t | $v_{\varphi 2}$ |
| 0.3 | 0.05 | -0.0202 |
| 0.5 | 0.05 | -0.0485 |
| 0.5 | 0.1 | -0.1818 |

$v_{\varphi 2}$ turns negative at a higher f and at a lower value of β , corresponding to $\dot{M} \sim 10^{-2} \dot{M}_{\text{Edd}}$.

V. DYNAMICS AND NATURE OF THE MAGNETIZED ACCRETION-INDUCED OUTFLOW

In this section, we analyze the family of solutions for advective flows in the accretion-outflow coupled region with $\dot{M} \lesssim 10^{-2} \dot{M}_{\text{Edd}}$. Although the flow variables vary in both r and z , we do not display three dimensional figures as they are very obscure and difficult to interpret. As outflow and jet effuse out from inner region of the accretion flow, we restrict our analysis up to 50 Schwarzschild radius (r_g) within which we presume that the accretion and outflow are coupled, where, $r_g = 2GM/c^2$. Also it has been stated by Kumar et al. (2013) that VLBI observations of M87 (Junor et al. 1999) have shown that the jet originates from the vicinity ($\sim 50r_g$) of a BH/compact object. However, we do not expect any outflow out of the accreting plasma in the extreme vicinity of a BH, as the accretion flow remains highly bounded in the extreme vicinity of a gravitationally starved BH. So we restrict our study up to $5r_g$ in the inward radial direction, a quite reasonable choice for the inner radius of the accretion-outflow coupled region. Both r and z coordinates in the figures are expressed in units of r_g . We express \dot{M} in our entire analysis in units of \dot{M}_{Edd} . The dynamical solutions are shown in the following figures with $G = M = 1$. Note that all the dynamical variables in our study are mean quantities, which are either time averaged or ensemble averaged. All the flow variables in the figures represent mean quantities.

Figures 1 and 2 describe the variation of vertically averaged flow variables as functions of radial coordinate r in different accretion paradigms. Variation of \bar{v}_z and \bar{B}_z are shown only along coupled accretion-outflow surface $h(r)$ as they are odd functions in z . Figure 1 shows that with the decrease in \dot{M} , the poloidal components of the velocity (\bar{v}_r, \bar{v}_z) and the sound speed consistently increases. Conversely, the magnitude of \bar{v}_φ increases with the flow becoming less advective and more centrifugally dominated. It is being interestingly found from the tables in §IV, that the value of the large-scale poloidal magnetic field enhances with the increase in the geometrical thickness of the accretion flow. As one moves from strongly advective regime to moderately advective regime, there is a sharp fall in the value of the poloidal component of the magnetic field. This is owing to the fact that the geometrical thickness of the accretion region corresponding to moderately advective accretion flow is much less as compared to the case in strongly advective accretion paradigm, as shown in figures 2a,b. This indicates the dominating influence of the vertical thickness of the accretion flow structure on the poloidal component of the magnetic field. In contrast, the toroidal component of the magnetic field \bar{B}_φ always increases with the flow becoming less advective and more centrifugally/rotationally dominated (Fig. 2c).

Figure 3 shows the variation of poloidal component of velocity and magnetic field with α for different accretion paradigms along the radial distance r . \bar{v}_r and \bar{B}_r are vertically averaged quantity, whereas \bar{v}_z and \bar{B}_z are along coupled accretion-outflow surface $h(r)$. We choose the value of corresponding t for different α to be maximum as illustrated in §IV. This is because the system has a greater tendency to relax itself to the maximum possible height available to render a physical plausible solution of the coupled accretion-outflow, as the geometrically thicker accretion flow is more conducive to propel plasma vertically outwards of the accretion region. We find that with a small increase in α from 0.3 to 0.5, the value of the poloidal component of velocity and the magnetic field increases for both accretion paradigms. We do not show the variation of other flow variables with α as their dependence on α is insignificant for a particular \dot{M} , which can be verified from tables in §IV.

In figures 4 and 5 we present the variation of the few dynamical variables in z (which are very relevant to outflow) at any arbitrary location in r , for $10^{-4} \dot{M}_{\text{Edd}} \lesssim \dot{M} \lesssim 10^{-2} \dot{M}_{\text{Edd}}$. Figure 4a shows the dependence of \bar{v}_z in z for different \dot{M} for $\alpha = 0.3$ similar to that in Fig. 1. It is found that initially \bar{v}_z increases rapidly in z , however there is a sudden deceleration of \bar{v}_z as the flow approaches the coupled accretion-induced outflow surface. This is due to the fact that

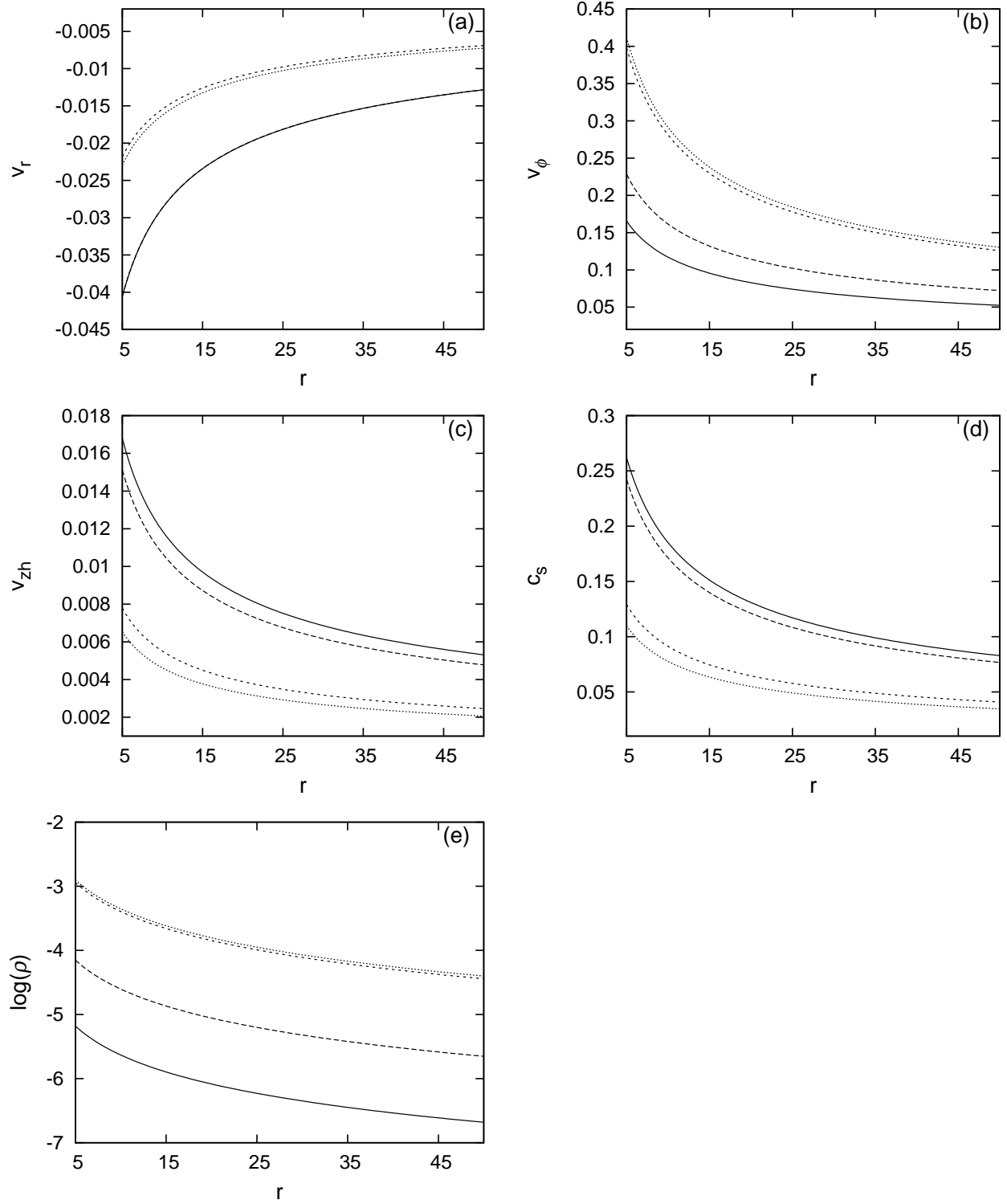


FIG. 1: Variation of (a) vertically averaged radial velocity, (b) vertically averaged toroidal velocity, (c) vertical/outflow velocity at height h , (d) vertically averaged sound speed, (e) vertically averaged density along radial coordinate r . r is expressed in units of Schwarzschild radius. Solid, long-dashed, short-dashed and dotted curves are for $(\dot{M} = 10^{-4}, 10^{-3}, 10^{-2}, 10^{-2})$ with corresponding $(f, \beta) = (0.1, 0.95), (0.1, 0.9), (0.4, 2/3), (0.5, 2/3)$, respectively. Other parameter is $\alpha = 0.3$. The flow variables in the vertical axis are in units of $\sqrt{GM/r_g}$, and density in units of $(GM)^{-1/2} \times \dot{M}_{\text{Edd}}/r_g^{3/2}$. \dot{M} is expressed in units of Eddington accretion rate.

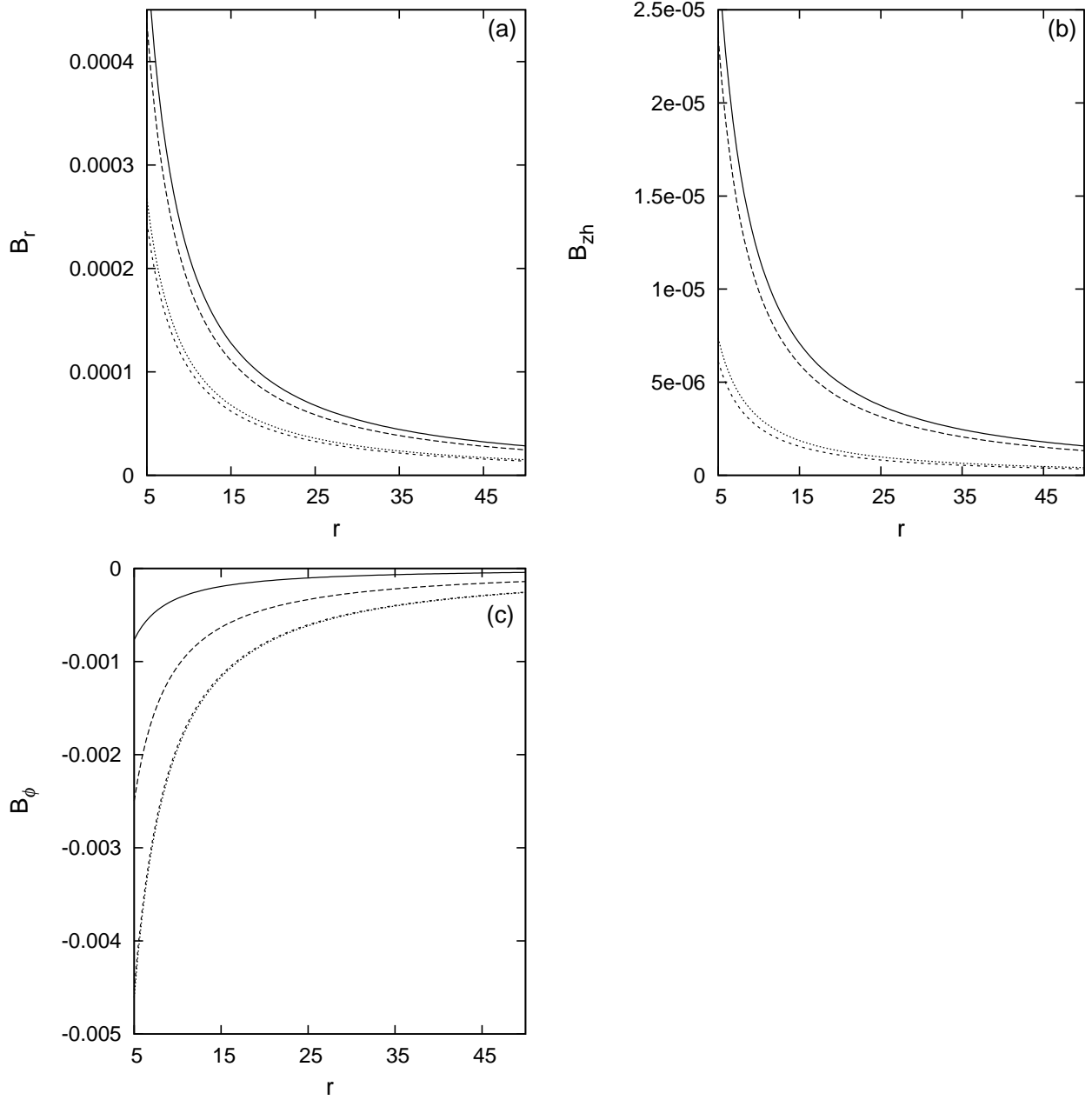


FIG. 2: Variation of (a) vertically averaged radial magnetic field, (b) vertically averaged toroidal magnetic field, (c) vertical magnetic field at h , along radial coordinate r . Solid, long-dashed, short-dashed and dotted curves are for $(\dot{M} = 10^{-4}, 10^{-3}, 10^{-2}, 10^{-2})$ with corresponding $(f, \beta) = (0.1, 0.95), (0.1, 0.9), (0.4, 2/3), (0.5, 2/3)$, respectively. Other parameter is $\alpha = 0.3$. r is expressed in units of Schwarzschild radius. Magnetic fields are in units of $(\sqrt{GM} \times \dot{M}_{\text{Edd}})^{1/2} / r_g^{5/4}$. \dot{M} is expressed in units of Eddington accretion rate.

the inward vertical component of the gravitational force (F_{Gz}) dominates near the coupled accretion-outflow surface. Also at low \dot{M} corresponding to moderately advective accretion flow, the increase of \bar{v}_z in the vertical direction is much steeper. The truncation of the curves at a particular z represent the corresponding vertical thickness t . Figure 4b shows the variation of \bar{v}_z in z with α for two different accretion paradigms similar to that in Fig. 3. The nature of the curves are similar to that in Fig. 4a. Nevertheless, with the increase in α , the value of \bar{v}_z gets enhanced, and there is a steeper increase of \bar{v}_z in z . The nature of the variation of toroidal component of the magnetic field in z for different \dot{M} is shown in Fig. 4c. It is seen that with the increase in \dot{M} , \bar{B}_φ increases at a much faster rate in z . Variation of \bar{B}_φ with α is insignificant (see tables in §IV) and hence is not graphically displayed. In figures 4d and 4e,

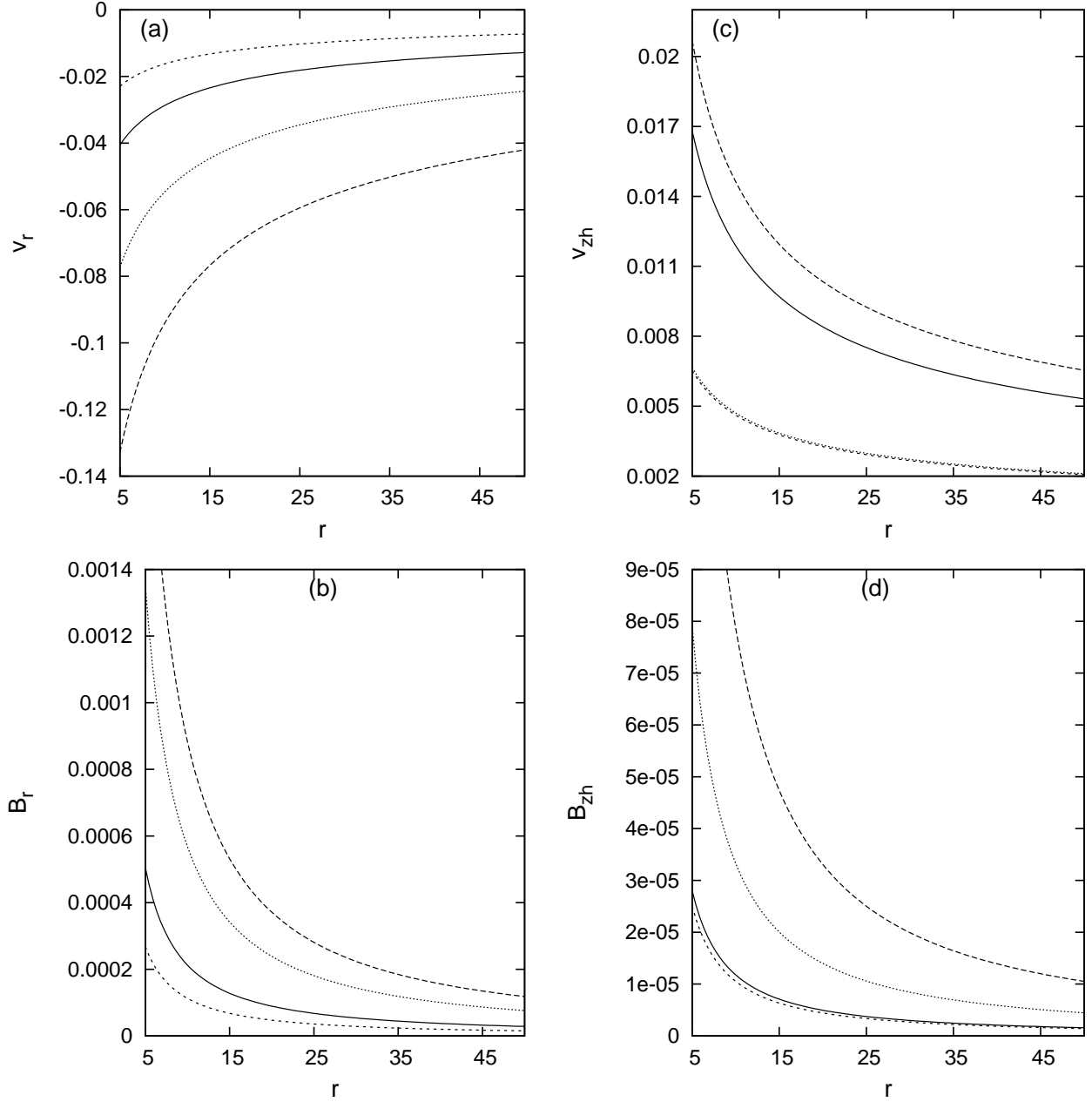


FIG. 3: Variation of poloidal components of velocity and magnetic field with α for two different accretion paradigms along r . Solid, long-dashed, short-dashed and dotted curves are for $(\dot{M}, \alpha, f, t) = (10^{-4}, 0.3, 0.1, 0.1), (10^{-4}, 0.5, 0.1, 0.2), (10^{-2}, 0.3, 0.5, 0.05), (10^{-2}, 0.5, 0.5, 0.1)$. The units of the variables along the axes are same as in figures 1 and 2. \dot{M} is expressed in units of Eddington accretion rate.

we show the variation of density in z corresponding to strongly advective and moderately advective accretion regimes, respectively. Both the figures indicate that $\bar{\rho}$ decreases with the increase in α for all \dot{M} . Also, there is a steeper fall of density in z with the increase in \dot{M} . Figure 5 depicts the variation of toroidal velocity \bar{v}_φ in z . With the increase in \dot{M} ($\dot{M} > 10^{-3} \dot{M}_{\text{Edd}}$) as the flow becomes less advective and more centrifugally dominated, \bar{v}_φ decreases in z for all relevant values of α and f . This feature of \bar{v}_φ has already been remarked in §IV. In figures 5c and 5d, we show them for $\dot{M} \sim 10^{-2} \dot{M}_{\text{Edd}}$. We also find that with increase in α the profile of \bar{v}_φ in z attains a steeper nature.

In figures 6b and 6a we depict the profile of differential magnetic torque ($-r^2 \bar{B}_\varphi \bar{B}_z$) along z , as well as differential magnetic torque acting on the coupled accretion-outflow surface ($-r^2 \bar{B}_{\varphi h} \bar{B}_{zh}$) along r , respectively, corresponding to different accretion paradigms. This term represents the magnetic extraction of angular momentum by the outflowing

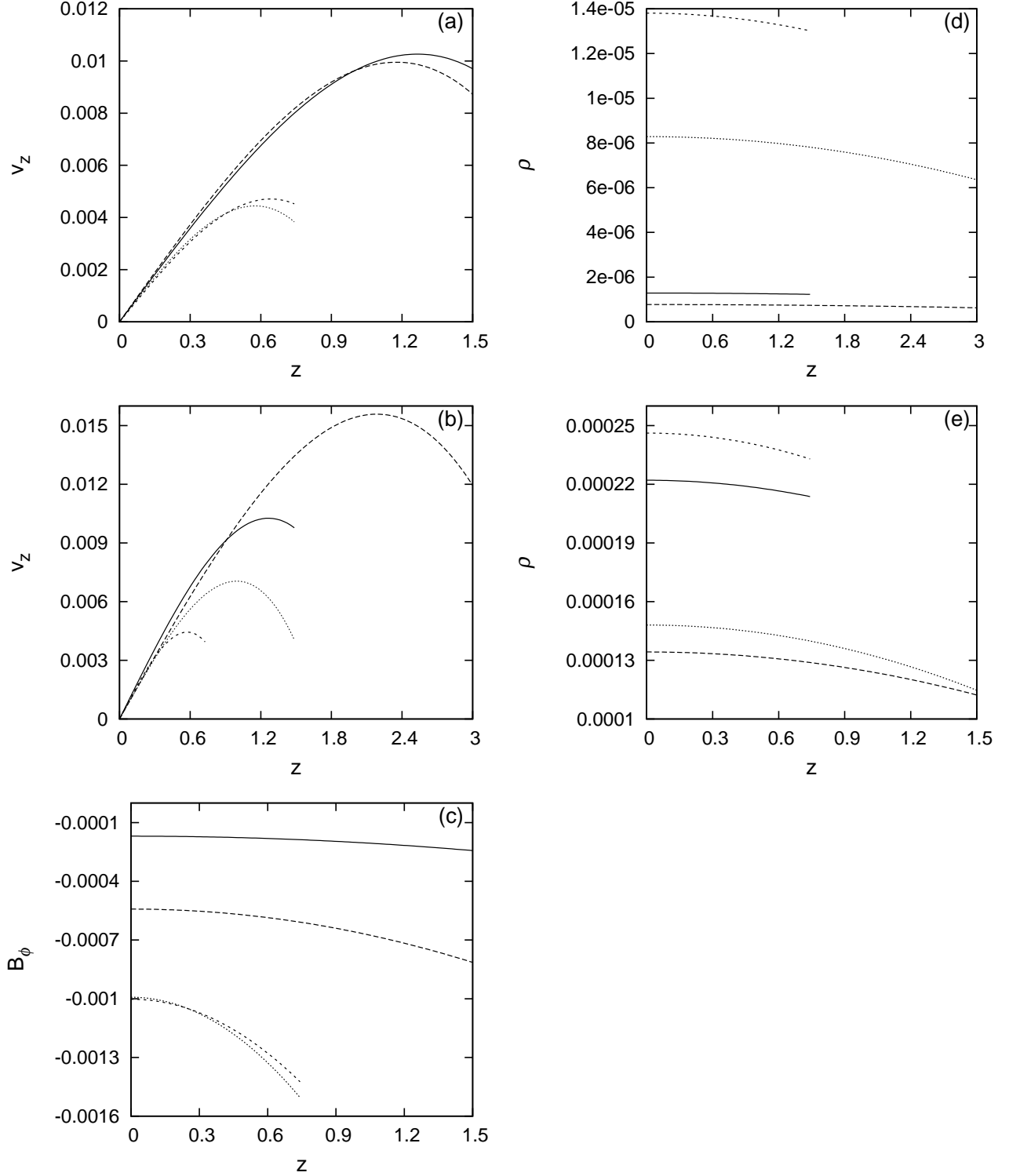


FIG. 4: Variation of flow variables along vertical coordinate z corresponding to $r = 15 r_g$. Solid, long-dashed, short-dashed and dotted curves in (a), (b) and (c) are for same parameters corresponding to figures 1, 3 and 1 respectively. Solid, long-dashed, short-dashed and dotted curves in (d) are for $(\dot{M}, \alpha, \beta, f) = (10^{-4}, 0.3, 0.95, 0.1), (10^{-4}, 0.5, 0.95, 0.1), (10^{-3}, 0.3, 0.9, 0.1), (10^{-3}, 0.5, 0.9, 0.1)$. Similarly the corresponding curves in (e) are for $(10^{-2}, 0.3, 2/3, 0.4), (10^{-2}, 0.5, 2/3, 0.4), (10^{-2}, 0.3, 2/3, 0.5), (10^{-2}, 0.5, 2/3, 0.5)$. The units of the variables along the axes are same as in figures 1 and 2 and 3. \dot{M} is expressed in units of Eddington accretion rate.

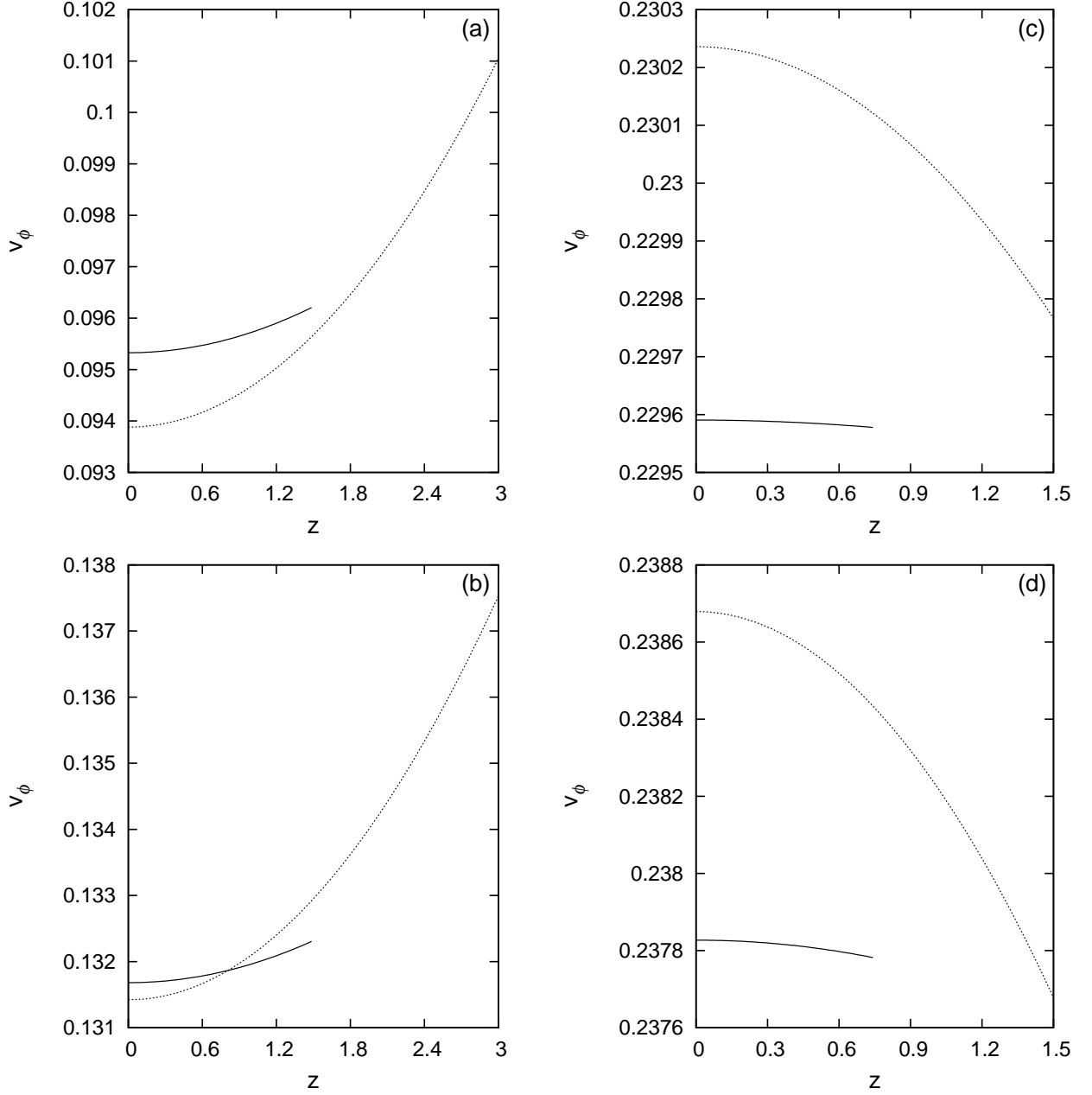


FIG. 5: Variation of toroidal velocity as a function of vertical coordinate z corresponding to $r = 15 r_g$. The solid and dotted curves are for $(\dot{M}, \alpha, \beta, f)$ in (a) $= (10^{-4}, 0.3, 0.95, 0.1)$, $(10^{-4}, 0.5, 0.95, 0.1)$, (b) $= (10^{-3}, 0.3, 0.9, 0.1)$, $(10^{-3}, 0.5, 0.9, 0.1)$, (c) $= (10^{-2}, 0.3, 2/3, 0.4)$, $(10^{-2}, 0.5, 2/3, 0.4)$, (d) $= (10^{-2}, 0.3, 2/3, 0.5)$, $(10^{-2}, 0.5, 2/3, 0.5)$. The units of variables along the axes are same as in earlier figures. \dot{M} is expressed in units of Eddington accretion rate.

matter, what is called the magnetic braking. The curves show that with the increase in the value of \dot{M} as well as with the increase in α (for a specific value of \dot{M}), the value of the differential magnetic torque increases. As \dot{M} increases, with the accretion flow becoming less advective and more centrifugally dominated, the extraction of angular momentum by the outflowing plasma is greatly enhanced. Consequently the gas gets centrifugally accelerated and would leave the accretion region by removing the angular momentum from the accreting matter. This mechanism predominantly determines the outward flow of the matter for accretion flow with moderate advection. If the system has a large residual toroidal velocity (centrifugally dominated), it is possible that the angular momentum loss in the vertical direction due to the magnetic torque will be so high, owing to which the degree of angular momentum loss proportionately increases as the matter flow vertically outwards. As a consequence, there will be an eventual decrease

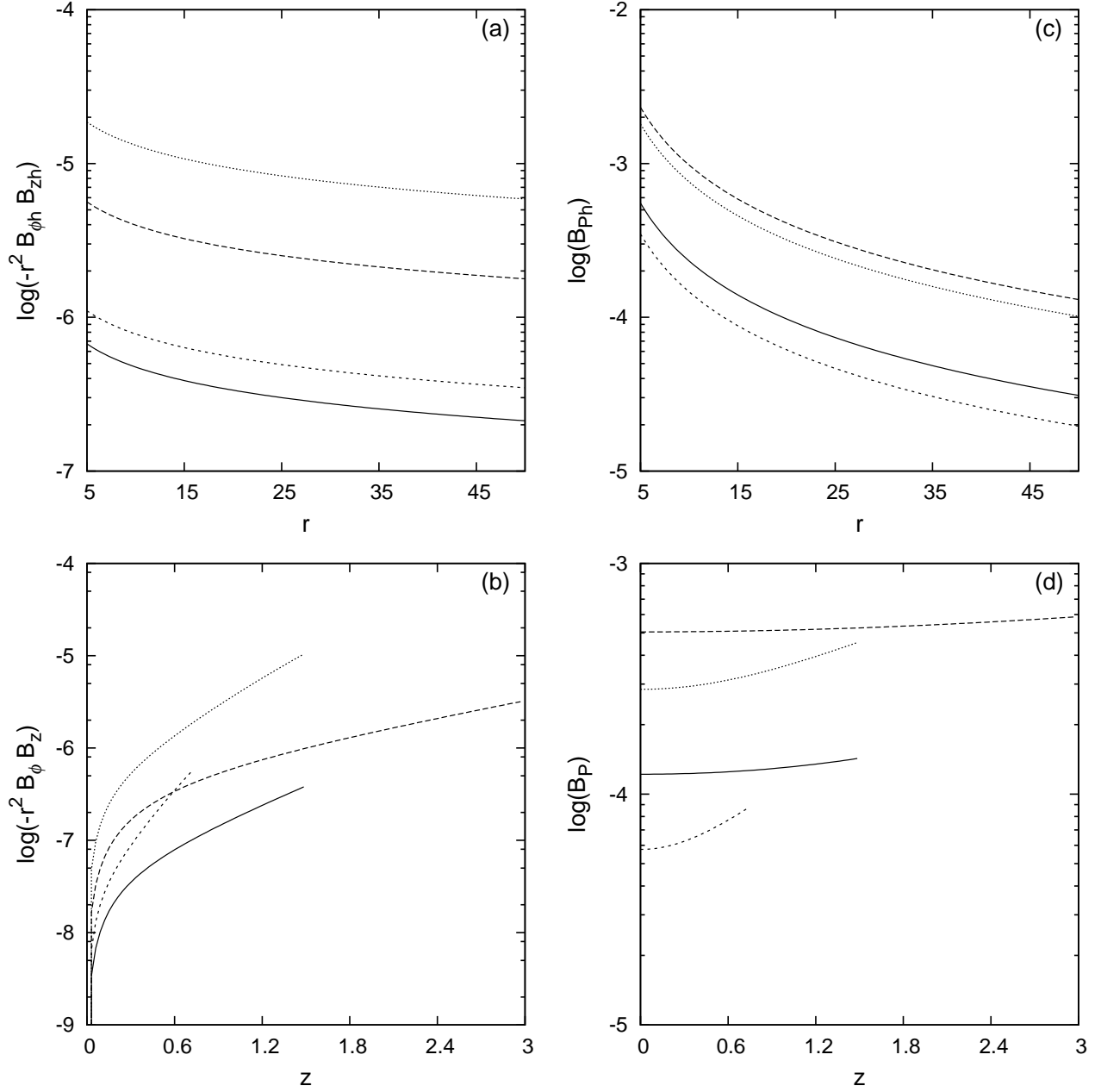


FIG. 6: Variation of differential magnetic torque and poloidal magnetic field along r and z . Variation along z is at $r = 15 r_g$. Solid, long-dashed, short-dashed and dotted curves in (a), (b), (c) and (d) are for $(\dot{M}, \alpha, f, t) = (10^{-4}, 0.3, 0.1, 0.1)$, $(10^{-4}, 0.5, 0.1, 0.2)$, $(10^{-2}, 0.3, 0.5, 0.05)$, $(10^{-2}, 0.5, 0.5, 0.1)$. The component of magnetic fields are expressed in units similar to earlier figures. r and z are expressed in units of Schwarzschild radius. \dot{M} is expressed in units of Eddington accretion rate.

of the toroidal velocity \bar{v}_ϕ in the vertical direction within the accretion-outflow coupled region, as seen in Fig. 5c,d, corresponding to accretion flow with $\dot{M} \sim 10^{-2} \dot{M}_{\text{Edd}}$. On the other hand, if the accretion flow is predominantly gas pressure dominated as in a strongly advective regime (with $\dot{M} \lesssim 10^{-3} \dot{M}_{\text{Edd}}$), the gas pressure gradient would play a more contributory role to lift the plasma vertically outwards with the help of magnetic forces, and the effective contribution of the magnetocentrifugal acceleration to control the dynamics of the outflowing matter gets curtailed as compared to that in a more centrifugally dominated accreting system.

Figures 6d and 6c show the variation of the poloidal component of the magnetic field $\bar{B}_P [= \sqrt{\bar{B}_r^2 + \bar{B}_z^2}]$ along z and at coupled accretion-outflow surface (\bar{B}_{Ph}) along r , respectively. The nature of the curves indicate that as high α renders the accretion-induced outflow to a greater geometrical thickness (commented earlier), the large-scale poloidal

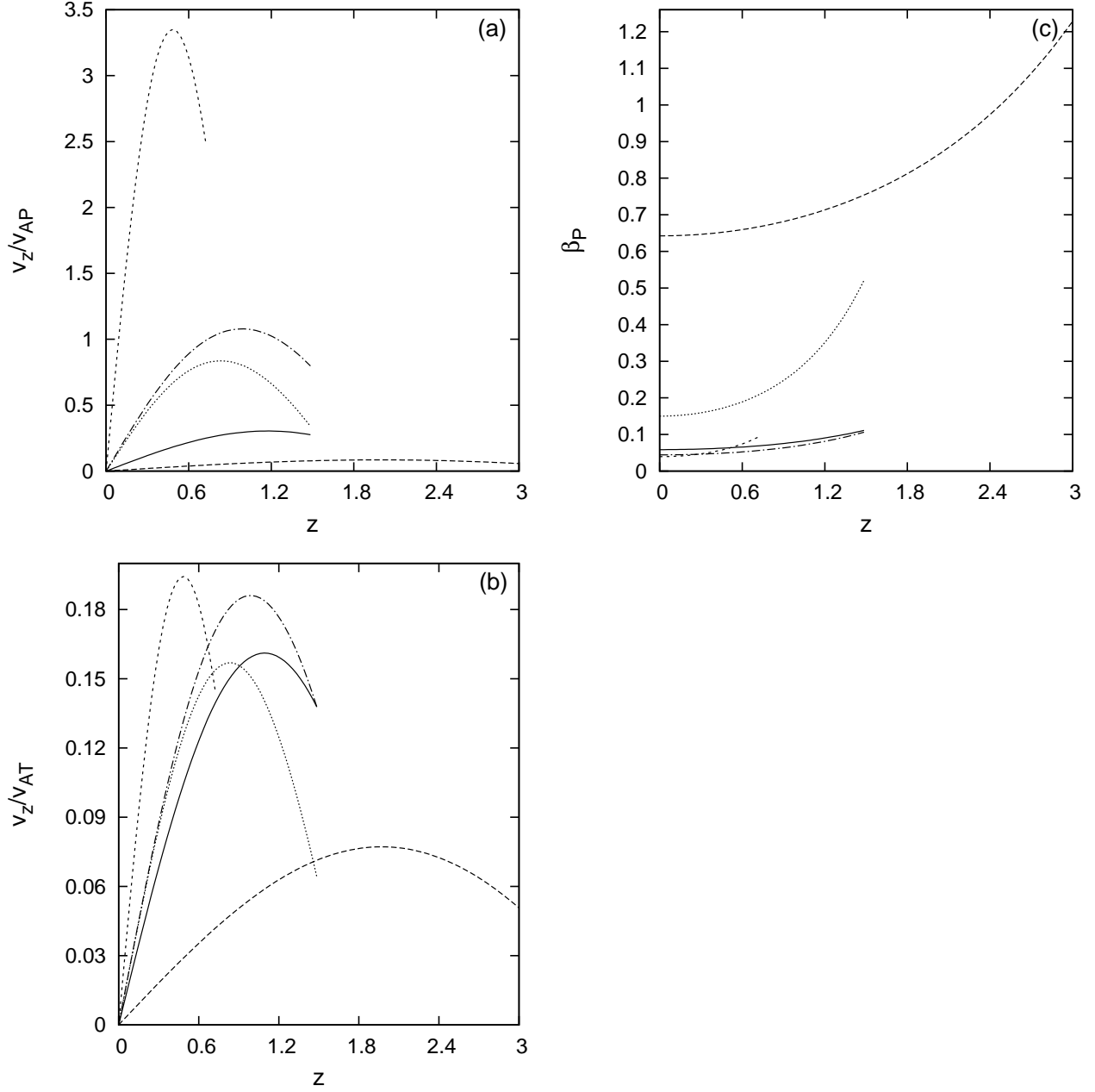


FIG. 7: Variation of the (a) ratio of vertical velocity to poloidal Alfvén velocity, (b) ratio of vertical velocity to total Alfvén velocity, (c) plasma β_P along z corresponding to $r = 15 r_g$. Solid, long-dashed, short-dashed, dotted, dot-dashed curves in (a), (b) and (c) are for $(\dot{M}, \alpha, f, t) = (10^{-4}, 0.3, 0.1, 0.1), (10^{-4}, 0.5, 0.1, 0.2), (10^{-2}, 0.3, 0.5, 0.05), (10^{-2}, 0.5, 0.5, 0.1), (10^{-3}, 0.3, 0.1, 0.1)$, \dot{M} is expressed in units of Eddington accretion rate.

field gets strongly augmented with the increase in α for a specific \dot{M} due to the dominating influence of the vertical thickness on \bar{B}_P . Thus with the increase in the turbulent viscosity parameter α , the value of the differential magnetic torque responsible for the centrifugal acceleration of the outflowing plasma, as well as the large-scale poloidal magnetic field \bar{B}_P get strongly augmented; consequently enhancing the transport of vertical flux outwards. In the moderately advective accretion paradigm with more centrifugal domination, the effective contribution to launch and eject the matter vertically outwards from the accretion region arises mainly from the magnetocentrifugal acceleration. A small increase in the turbulent viscosity parameter α from 0.3 to 0.5 intensifies the process of extraction of the angular momentum due to the magnetic torque. The eventual result is the enhanced transport of the outward vertical flux with the increase in the effective angular momentum transport in z direction. This renders v_{φ_2} to become negative

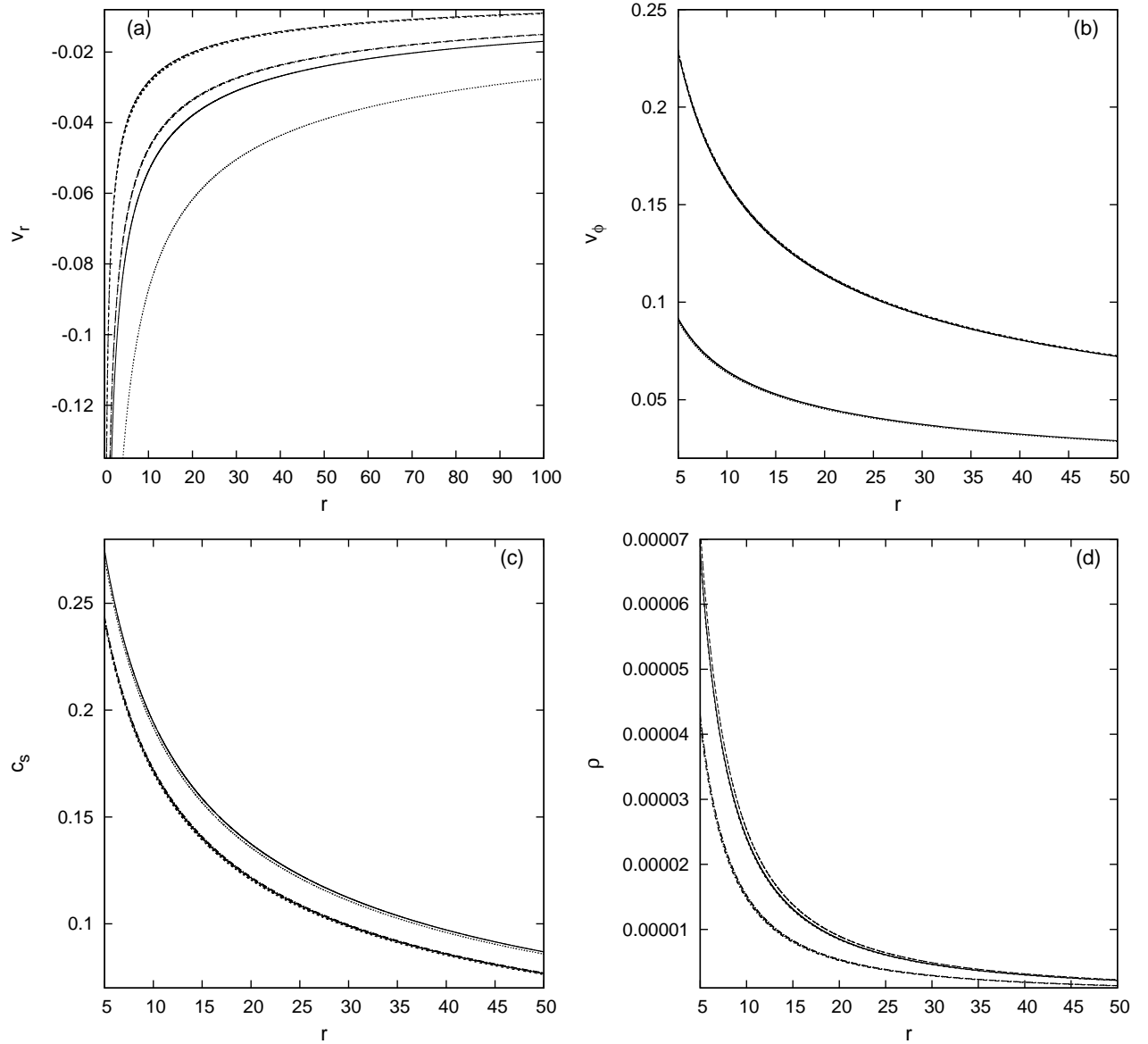


FIG. 8: Comparison of our magnetized accretion-outflow solutions with that of ADAF type solutions in Narayan & Yi 1994 [5]. In figures 8a,b,c,d we compare radial velocity, orbital velocity, sound speed and density, respectively, obtained for our magnetized accretion-outflow solutions with that of ADAF type solutions. The curves correspond to $\dot{M} = 10^{-3}$. Solid, long-dashed, short-dashed curves in all the figures corresponding to $\alpha = 0.3$. In all the figures, solid and long-dashed curves are for flow variables at equatorial plane corresponding to ADAF type and for our magnetized accretion-outflow solutions, respectively. Short-dashed curves correspond to flow variables for our magnetized accretion-outflow solution at height h . Long-dashed curves and short-dashed curves correspond to $t = 0.1$. Dotted, long dotted-dashed, short dotted-dashed curves exactly resemble solid, long-dashed and short-dashed curves, however correspond to $\alpha = 0.5$. Long dotted-dashed and short dotted-dashed curves correspond to equatorial plane and at scale-height h for our magnetized accretion-outflow solution, corresponding to $t = 0.1$. Other parameters are ($\beta = 0.9, f = 0.1$). \dot{M} is expressed in units of Eddington accretion rate. Velocities and density are expressed in units already stated in the caption in Fig. 1.

at a lower f and higher β as compared to that for $\alpha = 0.3$, as stated in last two lines of §4.3.

In Fig. 7a we show the variation of the ratio of \bar{v}_z and poloidal Alfvén velocity $\bar{v}_{AP} [= \bar{B}_P / \sqrt{4\pi\bar{\rho}}]$ in z for different \dot{M} and α . With the increase in \dot{M} as the system becomes less advective and more centrifugally/rotationally dominated, there is an increase in the ratio of \bar{v}_z / \bar{v}_{AP} . In contrast, with the increase in α for a specific \dot{M} there is a sharp fall in the value of the above ratio. Figure 7b shows the variation of the ratio of \bar{v}_z and net Alfvén velocity $\bar{v}_{AT} [= \bar{B} / \sqrt{4\pi\bar{\rho}}]$ in z similar to that in Fig. 7a. Figure 7c depicts the profile of plasma $\beta_P [= \bar{B}^2 / (8\pi\bar{\rho}c_s^2)]$ in z

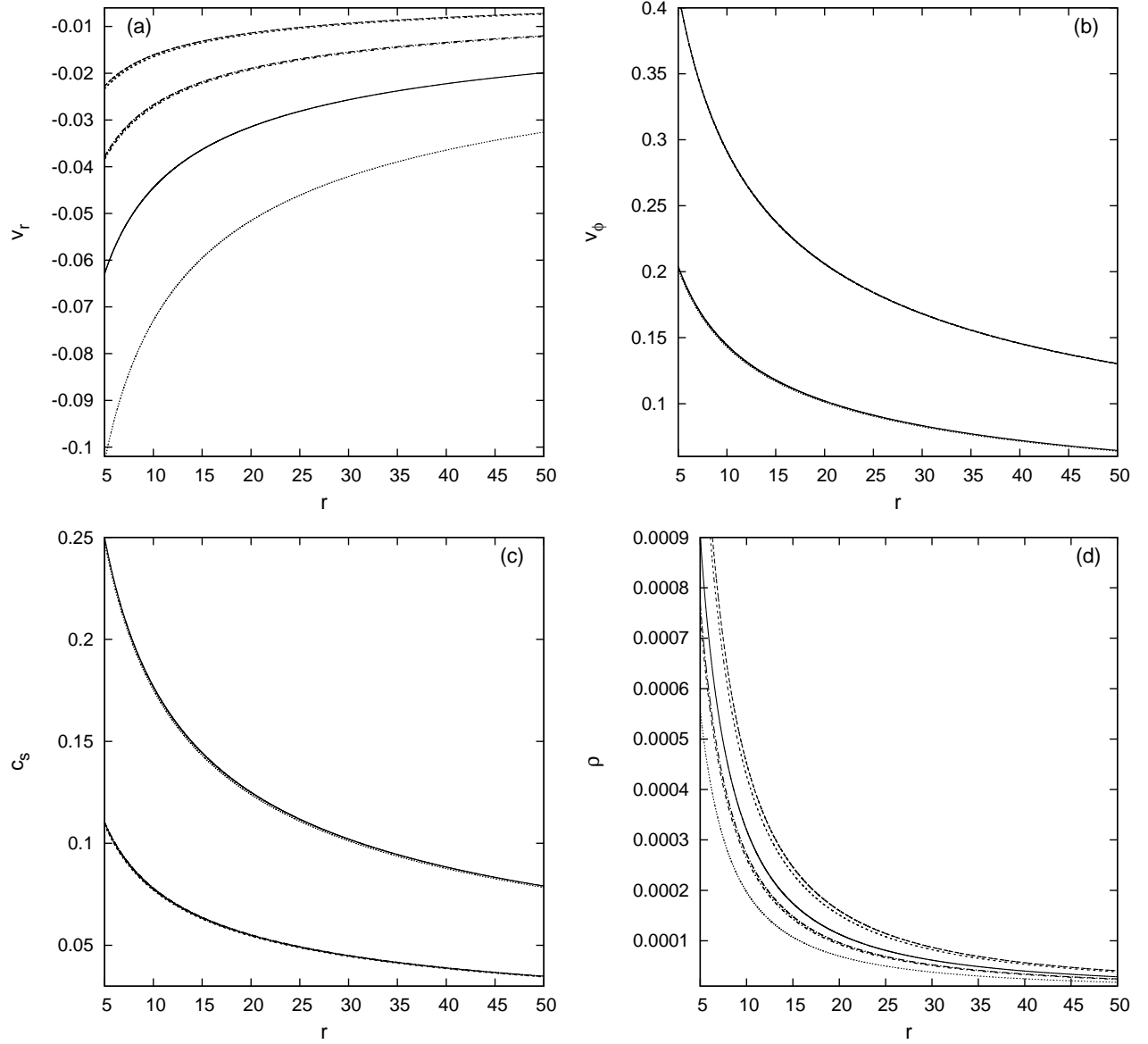


FIG. 9: Exactly similar to that of Fig. 8, however for $\dot{M} = 10^{-2}$. Solid, long-dashed, short-dashed curves in all the figures corresponding to $\alpha = 0.3$. Solid and long-dashed curves are for flow variables at equatorial plane corresponding to ADAF type and for our magnetized accretion-outflow solutions, respectively. Short-dashed curves correspond to flow variables for our magnetized accretion-outflow solution at height h . Long-dashed and short-dashed curves correspond to $t = 0.05$. Dotted, long dotted-dashed, short dotted-dashed curves resemble solid, long-dashed and short-dashed curves, however correspond to $\alpha = 0.5$. Long dotted-dashed and short dotted-dashed curves correspond to $t = 0.01$. Other parameters are ($\beta = 2/3, f = 0.5$). \dot{M} is expressed in units of Eddington accretion rate. Velocities and density are expressed in units already stated in the caption in Fig. 1.

for different \dot{M} and α . We find that β_P always increases steadily in the vertical direction, and its value gets strongly augmented with a small increase in α , however, it always remains mostly below equipartition for all relevant \dot{M} and α . Moreover it is found that with the increase in \dot{M} , in general, β_P decreases.

In figures 8 and 9 we make a comparison of our magnetized accretion-outflow solutions with that of ADAF type solutions in [5]. In figures 8 and 9, we compare the radial profiles for radial velocity, orbital velocity, sound speed and density, respectively, obtained for our magnetized accretion-outflow solutions with that of ADAF type solutions, corresponding to different \dot{M} and different α . We found that the magnitude of radial velocity along r that we obtained in our accretion-induced outflow is less as compared to that obtained in self-similar ADAF. On the other hand, the magnitude of orbital velocity along r obtained in our case is higher as compared to that obtained in ADAF. Also there

is a marginal decrease in the magnitude of sound speed or equivalently the temperature of the gas along r obtained in our accretion-induced outflow as compared to that obtained in ADAF. However, the magnitude of density of the gas along r in our accretion-induced outflow is found to be almost similar with that obtained in case of ADAF.

VI. DISCUSSION

Observationally it is found that low/hard state of BHXRBs which are supposed to be powered by geometrically thick strongly advective sub-Eddington (presumably with $\dot{M} \lesssim 10^{-3} \dot{M}_{\text{Edd}}$) and consequently quasi-spherical and radiatively inefficient accretion flows (RIAFs), emanate strong outflows and relativistic jets. Outflows and jets are not observed in high/soft of BHXRBs which are powered by geometrically thin and optically thick standard Keplerian accretion disk. The physics of origin and launching of outflows/jets in galactic BH systems (also called microquasars) is supposed to be similar with that corresponding to SMBHs in AGNs, as AGNs may be seen to be scaled up galactic BHs [37]. Geometrically thick advective accretion flow having substantial amount of gas pressure with strong advection, is more conducive to effuse and accelerate plasma in the vertical direction out of the inner accretion region. Although we do not aspire to explore the exact mechanism of launching and ejection of jets, however, it is generally conceived that the origin, launching and ejection of outflow and jet from the accretion flow is a magnetohydrodynamic process. In the present work we mainly focussed on accretion powered hydromagnetic outflows.

Although the distinctive cause of the origin and launching of accretion powered hydromagnetic outflows is still inconclusive, however, it is certain that the dynamics of the outflowing matter should be intrinsically coupled to the accretion dynamics through the fundamental laws of conservation of (matter, momentum and energy) within the coupled accretion-induced outflow region, and should not be treated as dissimilar objects. Conservation laws are the most valuable foundation in physics, and play a significant role in understanding astrophysical outflows and jets. This is because the physical dynamics of the coupled inflow and outflow are essentially governed by the laws of conservation. The nature of the dynamical solutions in the accretion-outflow coupled region should then reflect upon the physical conditions/criteria to eject outflows. For the theoretical analysis of the accretion-outflow coupling one needs to be very thoughtful about the proper modelling of the system which essentially needs to solve a complete set of magnetohydrodynamic conservation equations in 2.5-dimension viscous, resistive, advective paradigm. In §II we have endeavoured to describe a robust form of accretion-outflow coupled magnetohydrodynamic set of equations in viscous, resistive, advective paradigm, upholding all the conservation laws in 2.5-dimensional mean field MHD regime without any ad hoc proposition, where the dynamical flow variables vary in (r, z) . The mean field approximation gives rise to the emergence of various turbulent correlation terms, where we restrict our study to first order turbulent correlation. Note that turbulent magnetic diffusivity and turbulent viscous term in induction and energy conservation equation arises only from the kinetic part of the turbulent stress tensor through the Reynolds stress. In this work, we have assumed isotropic turbulence and also neglected the contribution of other turbulent stress tensors apart from $r\varphi$, which may be dynamically important. The contribution $r\varphi$ component would be dynamically more dominant as is responsible for the radial transport of angular momentum outwards. Vertical transport of angular momentum occurs mainly through large-scale magnetic stresses. Nonetheless, in future we would like to examine the possibility of their inclusion, as well as investigate the nature of the flow with anisotropic turbulence.

The inflow and outflow are governed by eight coupled integro-partial differential MHD equations in the cylindrical geometry. Limited observational inputs put constraint on the boundary conditions as well as the scaling relation between accretion and the outflow. Owing to the fact that it is beyond the scope to have complete global numerical solutions of the said coupled partial differential MHD equations, motivated us to invoke necessary and proper quasi-analytical method to solve them. Ever since the work of [5], use of power law self-similarity in studying the accretion flow dynamics, especially the advection dominated accretion flows (ADAFs) to explain the nature of LLAGNs has become widely popular. Realistic strongly advective accretion flow preserves self-similarity reasonably well, within an appreciable region of the flow [5,38], and has been widely used to explain observational features in LLAGNs (see [39] for a review). Previously, self-similar methods had been indeed used to study outflow from the accretion disk on many occasions (see the references in §I in introduction). It is being found from many studies that self-similarity holds approximately well in context to outflows [40,18,28,29,41]. Keeping the essence of power law self-similarity, we sought a generalized n^{th} degree polynomial expansion of all the dynamical variables in two dimensions, and solve the complete set of coupled integro-partial differential MHD conservation equations within the accretion-outflow coupled region self-consistently, in 2.5 dimensional viscous, resistive advective paradigm, where we have restricted up to order $[h(r)/r]^2$.

In sections 4 and 5, we have analyzed the nature and the behaviour of our MHD solutions in advective accretion paradigm with $\dot{M} \lesssim 10^{-2} \dot{M}_{\text{Edd}}$. Although we have not intended to explore the physical mechanism of outflow/jet

launching in the present study, the quasi-stationary dynamical solutions of the accretion-induced outflow carry the information about the physical conditions/criteria to propel matter vertically outwards out of the accretion-outflow region. We have mainly focused within the accretion-outflow coupled region where the flow is essentially bounded. We obtain solutions at a reduced vertical thickness irrespective of the nature of accretion paradigm which we have focused on. Magnetic field tends to compress or squeeze the accretion region by counterbalancing the thermal pressure gradient. We found that the large-scale poloidal component of the magnetic field is enhanced with the increase in the geometrical thickness of the accretion flow, consistently. With the increase in \dot{M} as $10^{-4}\dot{M}_{\text{Edd}} \ll \dot{M} \lesssim 10^{-2}\dot{M}_{\text{Edd}}$, with the accretion flow becoming less advective and more centrifugally dominated with lesser geometrical thickness i.e., for the flow with moderate advection, there is a sharp fall in the value of poloidal component of the magnetic field, however with a strong enhancement in the value of the toroidal component of the magnetic field and consequently the differential magnetic torque ($-r^2\bar{B}_\varphi\bar{B}_z$). This term (differential magnetic torque) is responsible for the magnetic extraction of the angular momentum to magnetocentrifugally accelerate the outflowing plasma out of the radial accretion flow, and this predominantly determines the outward flow of the matter in a moderately advective accretion paradigm which is more centrifugally dominated. However, with the decrease in \dot{M} as the flow becomes strongly advective ($\dot{M} \lesssim 10^{-3}\dot{M}_{\text{Edd}}$) and geometrically more thick with strong gas pressure and inefficient cooling, despite in the decrease in the value of $-r^2\bar{B}_\varphi\bar{B}_z$, a consistent increase in the v_z occurs, indicating that the gas pressure gradient might play a more contributory role to lift the plasma vertically outwards with the help of magnetic forces. The plasma in the accretion flow can be lifted outwards and ejected, only if some physical process can overcome the effect of the inward vertical force due to the central gravity. The dynamical behaviour of the solutions indicate that in the advective paradigm both magnetocentrifugal acceleration and thermal pressure gradient along with the magnetic forces, will help in lifting and accelerating the plasma vertically outwards, and the gas material will diffuse outwards across magnetic field lines. However, the effective contribution of either magnetocentrifugal acceleration or thermal pressure gradient to lift the plasma vertically outwards depends on the degree to which the flow is advective. In fact, with the increase in mass accretion rate as the flow tends to become less advective and more centrifugally dominated with lesser geometrical thickness, in general, the efficacy of the disk to eject outflows diminishes. In paper II (in preparation), we have quantitatively demonstrated this aspect with the increase in \dot{M} from $10^{-4}\dot{M}_{\text{Edd}}$ to $10^{-2}\dot{M}_{\text{Edd}}$; the accretion flow with $\dot{M} \sim 10^{-2}\dot{M}_{\text{Edd}}$, least conducive to eject outflows.

We obtain dynamical solutions in accretion-outflow coupled region only at high turbulent diffusive parameter $\alpha (\gtrsim 0.3)$. The accretion-induced outflow solutions have a profound dependence on turbulent diffusive parameter α . It is being interestingly found from our solutions that the enhancement in α renders the accretion-induced outflow region to attain a greater geometrical thickness. Consequently, the poloidal component of magnetic field \bar{B}_P , as well as the differential magnetic torque ($-r^2\bar{B}_\varphi\bar{B}_z$) get strongly augmented, enhancing the transport of vertical flux outwards. Also the plasma beta β_P increases steadily in the vertical direction, and its value gets strongly augmented with a small increase in α , however, it always remains mostly below equipartition within the accretion-outflow coupled region. Although we expect the accretion flow to have a large α owing to advective nature of the flow, however, the values of α that we have obtained in our solution may have been slightly overestimated. Nonetheless, it is indeed being found from previous works [5,6,38,42] that strongly advective accretion flows, in general, are mostly plausible for large values of α ($\alpha \gtrsim 0.1$). Gu and Lu [43] also shown that the transition from an outer geometrically thin Keplerian disk to an advection-dominated accretion flow is possible for $\alpha > 0.5$. McKinney and Narayan [29], in their GRMHD simulation of disk-outflow model, found to have large turbulent viscosity parameter in the accretion disk in the vicinity of the BH. Further, King, Pringle and Livio [44] suggested a typical range of $\alpha \sim (0.1 - 0.4)$ from observational evidence.

One of the important approximation we have used in our study is to treat the scale-height of accretion-outflow coupled region as a parameter. In reality the physical conditions to launch outflow would consistently determine the vertical height of the inflow-outflow surface, from where the outflow decouples from the accretion region. Moreover, in our study we have neglected the effect of spin of the BH in the accretion dynamics and its subsequent impact on the outflow, as the self-similar technique can only be used in the Newtonian approximation. This restricts us of using this method to investigate the physical behaviour of the system in the extreme vicinity of the BH, where general relativistic effects are indispensable. Although power law self-similarity is an analytical approximation, and the quantitative feature of the solutions may have been either overestimated or undervalued, the dynamical solutions show consistent and predictable behaviour, and do exhibit many physical insights on the nature of the accretion-induced outflow, as well reflect upon the relevant physical conditions to propel and eject plasma out of the accretion flow. Power law self-similarity, thus, seems to be reasonably good approximation, within the accretion-outflow coupled region.

Nonetheless, more extensive study is required to understand the definitive criteria or condition in launching accretion powered outflows and jets. BH spin is a very important aspect that needs to be incorporated in the conservation equations atleast through the use of pseudo-Newtonian potentials (e.g., [45]), while understanding accretion powered

outflow dynamics or the correlated dynamics of accretion and outflow. It is found from the work of [10] that the spin of the BH significantly influences accretion powered outflows/jets; for a rapidly rotating BH, the outflow power increases by \sim two orders in magnitude. Moreover, it is also essential that to have complete and a more realistic understanding of the dynamics of the accretion-outflow coupled region, a global numerical solution of such a system in advective paradigm should be performed. Also, explicit inclusion of cooling/radiative processes is required for the completeness of energy conservation. The relevant dynamical solutions at the accretion-outflow coupled surface would then necessarily act as boundary conditions at the base of the jet. A more definitive understanding of the criteria to launch accretion powered outflows and jets, thus, requires a complete 2.5-dimensional viscous, resistive, advective global MHD numerical solution with the inclusion of BH spin, which is left for future work. In a subsequent work [paper II (in preparation)] we will investigate in detail, the energetics of the magnetized accretion-induced outflows and study the spectral behaviour of accretion powered sources.

Appendix A

The integro-differential continuity equation (7), after substitution of the flow variables in the n^{th} polynomial order is given by

$$\sum_{n=0}^{\infty} \left[\frac{1}{2n+1} \sum_{m=0}^n \rho_{2(n-m)} v_{r2m} + \frac{1}{e+c-2n+2} \sum_{m=0}^n \rho_{2(n-m)} v_{z(2m+1)} \right] \left(\frac{h}{r} \right)^{2n+1} = -\frac{\dot{M}}{4\pi} \quad (\text{A1})$$

Similarly the polynomial expansion of all the other height-integrated MHD equations are done, however we do not furnish all of them here as the structure of the equations are huge. As an example we show it for the radial momentum balance equation (9).

$$\begin{aligned} & \left[\sum_{n=0}^{\infty} \sum_{m=0}^n \sum_{l=0}^m (a-2l) \rho_{2(n-m)} v_{r2(m-l)} v_{r2l} - \sum_{n=0}^{\infty} \sum_{m=0}^n \sum_{l=0}^m \rho_{2(n-m)} v_{\varphi2(m-l)} v_{\varphi2l} \right. \\ & + \sum_{n=1}^{\infty} \sum_{m=1}^n \sum_{l=1}^m 2l \rho_{2(n-m)} v_{z[2(m-l)+1]} v_{r2l} + GM \sum_{n=0}^{\infty} \sum_{m=0}^n \left(\frac{-3/2}{m} \right) \rho_{2(n-m)} \\ & + \sum_{n=0}^{\infty} \sum_{m=0}^n \sum_{l=0}^m (e-2n+2d) \rho_{2(n-m)} c_{s2(m-l)} c_{s2l} + \frac{1}{4\pi} \left[\sum_{n=0}^{\infty} \sum_{m=0}^n (j-2m+1) B_{\varphi2(n-m)} B_{\varphi2m} \right. \\ & \left. + \sum_{n=1}^{\infty} \sum_{m=1}^n [k-2(m-1)] B_{z[2(n-m)+1]} B_{z[2(m-1)+1]} - \sum_{n=1}^{\infty} \sum_{m=1}^n 2m B_{z[2(n-m)+1]} B_{r2m} \right] \left. \right] \frac{1}{2n+1} \left(\frac{h}{r} \right)^{2n} = 0. \quad (\text{A2}) \end{aligned}$$

-
- [1] I. F. Mirabel, L. F. Rodriguez, *Nature*, **371**, 46 (1994); I. F. Mirabel, L. F. Rodriguez, *Nature*, **392**, 673 (1998); S. S. Eikenberry, K. Matthews, E. H. Morgan, R. A. Remillard, R. W. Nelson, *ApJ*, **494**, 61 (1998)
 - [2] R. D Blandford, M. J. Rees, *MNRAS*, **169**, 395 (1974); M. C. Begelman, R. D. Blandford, M. J. Rees, *RvM*, **56**, 255 (1984); I. F. Mirabel, *New Ast. Rev.*, **47**, 471 (2003)
 - [3] R. P. Fender, T. M. Belloni, E. Gallo, *MNRAS*, **355**, 1105 (2004)
 - [4] A. Rushton, R. Spencer, R. Fender, G. Pooley, *A&A*, **524**, 29 (2010)
 - [5] R. Narayan, I. Yi, *ApJ*, **428**, 13 (1994)
 - [6] R. Narayan, I. Yi, *ApJ*, **452**, 710 (1995)
 - [7] N. I. Shakura, R. A. Sunyaev, *A&A*, **24**, 337 (1973); J. Frank J, A. R. King, D. J. Raine, *Accretion Power in Astrophysics*, (third, edition, Cambridge, UK: Cambridge University Press), (2002)
 - [8] S. Ghosh, B. Mukhopadhyay, *RAA*, **9**, 157 (2009)
 - [9] S. Ghosh, B. Mukhopadhyay, V. Krishan, M. Khan, *New Astron*, **15**, 83 (2010)
 - [10] D. Bhattacharya D, S. Ghosh, B. Mukhopadhyay, *ApJ*, **713**, 105 (2010)
 - [11] D. L. Meier *ApJ*, **522**, 753 (1999); D. R. Ballantyne, A. C. Fabian, *ApJ*, 622, 97 (2005)

- [12] S. W. Allen, R. J. H. Dunn, A. C. Fabian, G. B. Taylor, C. S. Reynolds, MNRAS, **372**, 21 (2006); M. J. Hardcastle, D. A. Evans, J. H. Croston, MNRAS, **370**, 1893 (2006); M. J. Hardcastle, D. A. Evans, J. H. Croston, MNRAS, **376**, 1849 (2007); B. Balmaverde, R. D. Baldi, A. Capetti, A&A **486**, 119 (2008); S. Ghosh, P. Banik, IJMPD, **24**, 1550084 (2015)
- [13] R. Narayan, F. Yuan, ARA&A, **52**, 529 (2014)
- [14] B. Czerny, B. You, 2015, *arXiv:150705852* (2015)
- [15] R. D. Blandford, D. G. Payne, MNRAS, **199** 883 (1982)
- [16] R. E. Pudritz, C. A. Norman, ApJ, **301**, 571 (1986)
- [17] M. Wardle, A. Königl, ApJ, **410**, 218 (1993); J. Contopoulos J, ApJ, **460**, 185 (1996); J. Ferreira J, G. Pelletier, A&A, **295**, 807 (1995); J. Ferreira, A&A, **319**, 340 (1997); F. Casse F, J. Ferreira, A&A, **353**, 1115 (2000); R. Narayan, J. C. McKinney, A. J. Farmer, MNRAS, **375**, 548 (2007)
- [18] R. E. Pudritz, R. Ouyed, Ch. Fendt, A. Brandenburg, prpl.conf, Protostars and Planets, V, B. Reipurth, D. Jewitt, and K. Keil (eds.), University of Arizona Press, Tucson, **951** 277 (2007)
- [19] G. S. Bisnovatyi-Kogan, R. V. E. Lovelace, ApJ, **529**, 97 (2000)
- [20] E. M. de Gouveia dal Pino, A. Lazarian, A&A, **441**, 845 (2005); E. M. de Gouveia dal Pino, P. P. Piovezan, L. H. S. Kadowaki, A&A, **518**, 5 (2010); D. Giannios, D. A. Uzdensky, M. C. Begelman, MNRAS, **402**, 1649 (2010)
- [21] A. Merloni, S. Heinz, T. di Matteo, MNRAS, **345**, 1057 (2003)
- [22] R. P. Fender, T. M. Beloni, ARA&A, **42**, 317 (2004)
- [23] F. Yuan F, W. Cui, R. Narayan, ApJ, **620**, 905 (2005); E. G. Körding, S. Migliari, R. Fender, T. Belloni, C. Knigge, I. McHardy, MNRAS, **380**, 301 (2007); J. Neilsen, J. C. Lee, Nature, **458**, 481 (2009); P. Soleri et al., MNRAS, **406**, 1471 (2010); J. C. A Miller-Jones et al., IAUS, **275**, 224 (2011); J. C. A Miller-Jones et al., MNRAS, **421**, 468 (2012); J. J. Miller et al. ApJ, **776**, 104 (2013); A. L. King, J. M. Miller, M. T. Reynolds, K. Gültekin, E. Gallo, D. Maitra, ApJ, **774**, 25 (2013)
- [24] R. D. Blandford, M. C. Begelman, MNRAS, **303**, 1 (1999)
- [25] R. Soria, J. Li, D. T. Wickramasinghe, ApJ, **487**, 769 (1997)
- [26] M. Samadi, S. Abbassi, MNRAS, **455**, 3381 (2016)
- [27] K.-I. Nishikawa et al. ApJ, **625**, 60 (2005)
- [28] J. C. McKinney, R. Narayan MNRAS, **375**, 531 (2007)
- [29] J. C. McKinney, R. Narayan MNRAS, **375**, 513 (2007)
- [30] F. Casse, R. Keppens ApJ, **601**, 90 (2004)
- [31] F. Krause, K. H. Rädler, *Mean Field Magnetohydrodynamics and Dynamo Theory*, Pergamon Press, (1980)
- [32] M. E. Pessah, C. Chan, D. Psaltis, PhRvL, **97**, 1103 (2006)
- [33] R. V. E. Lovelace, J. C. L. Wang, M. E. Sulkanen, ApJ, **315**, 504 (1987)
- [34] M. E. Pessah, C. Chan, D. Psaltis, MNRAS, **372**, 183 (2006)
- [35] R. Kumar, C. B. Singh, I. Chattopadhyay, S. K. Chakrabarti, MNRAS, **436**, 2864 (2013)
- [36] W. Junor, J. A. Biretta, M. Livio, Nature, **401**, 891 (1999)
- [37] I. M. McHardy, E. Koerding, C. Knigge, P. Uttley, R. P. Fender, Nature, **444**, 730 (2006); E. Körding, H. Falcke, S. Corbel, A&A, **456**, 439 (2006)
- [38] R. Narayan, S. Kato, F. Honma, ApJ, **476**, 49 (1997)
- [39] L. C. Ho, ARA&A, **46**, 475 (2008)
- [40] C. Fendt, ApJ, **651**, 272 (2006)
- [41] M. Stute, J. Gracia, N. Vlahakis, K. Tsinganos, A. Mignone, S. Massaglia, MNRAS, **439**, 3641 (2014)
- [42] F. Yuan, R. Ma, R. Narayan, ApJ, **679**, 984 (2008)
- [43] Wei-Min Gu, Ju-Fu Lu, 2000, ApJL, **540**, 33 (2000)
- [44] A. R. King, J. E. Pringle, M. Livio, MNRAS, **376**, 1740 (2007)
- [45] S. Ghosh, B. Mukhopadhyay, ApJ, **367**, 667 (2007); S. Ghosh, T. Sarkar, A. Bhadra, Phys. Rev. D, **92**, 083010 (2015); T. Sarkar, S. Ghosh, A. Bhadra, Phys. Rev. D, **90**, 063008 (2014); S. Ghosh, T. Sarkar, A. Bhadra, ApJ, **828**, 6 (2016)